Isogeometric collocation for implicit dynamics of three-dimensional beams undergoing finite motions

Enzo Marino[a,*], Josef Kiendl[b], Laura De Lorenzis[c]

[a]*Department of Civil and Environmental Engineering – University of Florence, Via di S. Marta 3, 50139 Firenze, Italy.*
[b]*Department of Marine Technology – Norwegian University of Science and Technology, NO-7491 Trondheim, Norway.*
[c]*Institute of Applied Mechanics – TU Braunschweig, Pockelsstraße 3, 38106 Braunschweig, Germany.*

Abstract

We propose a novel approach to the implicit dynamics of shear-deformable geometrically exact beams, based on the isogeometric collocation method combined with the Newmark time integration scheme extended to the rotation group SO(3). The proposed formulation is fully consistent with the underlying geometric structure of the configuration manifold. The method is highly efficient, stable, and does not suffer from any singularity problem due to the (material) incremental rotation vector employed to describe the evolution of finite rotations. Consistent linearization of the governing equations, variables initialization and update procedures are the most critical issues which are discussed in detail in the paper. Numerical applications involving very large motions and different boundary conditions demonstrate the capabilities of the method and reveal the critical role that the high-order approximation in space may have in improving the accuracy of the solution.

Keywords: Isogeometric collocation, Implicit dynamics, Geometrically nonlinear Timoshenko beams, Finite rotations, Newmark method

1. Introduction

For many complex engineering problems nonlinear beam models, able to accurately reproduce large three-dimensional motions, are often the preferred choice due the low computational cost compared to higher-dimensional models. In pursuing increased efficiency,

*Corresponding author
Email address: `enzo.marino@unifi.it` (Enzo Marino)

robustness and geometric capabilities with respect to existing methods, in this work for the first time the isogeometric collocation (IGA-C) method is used to solve the implicit dynamic problem of geometrically exact beams employing the Newmark time integration scheme extended to the rotation group SO(3). The IGA-C method was proposed in [1, 2] with the aim of exploiting the higher smoothness of NURBS basis functions used in isogeometric analysis (IGA) [3, 4] and the low computational cost of collocation. In IGA higher-order basis functions with tailorable smoothness, used both for the geometry representation and the space discretization of the differential problem, have proven to achieve increased accuracy and robustness on a per degree-of-freedom basis compared with standard Finite Element Analysis (FEA) [5–8]. Moreover, mesh generation and refinement are significantly simplified and, once the initial mesh is generated, refinements do not affect the geometric approximation. High-order basis functions require a larger number of quadrature points causing a fast growth of the computational cost. Countermeasures against this limitation are still being investigated, although significant progress has been made in [9–13]. IGA-C represents an extreme remedy since the need for numerical quadrature is completely removed due to the discretization of the strong form of the governing equations. IGA-C requires only one evaluation point per degree of freedom, regardless of the approximation degree, resulting in a much faster method compared to standard Galerkin-based IGA [14].

IGA-C proved excellent performances in a wide range of applications, such as linear problems [1, 2, 14], phase-field modeling [15], contact problems [16, 17], hyperelasticity [17]. New relations between Galerkin and collocation methods were found in [18]. Timoshenko beam formulations were successfully proposed in [19–23]. Bernoulli-Euler beams and Kirchhoff plates were addressed in [24], and Reissner-Mindlin plate and shell problems in [25] and [26], respectively. Kirchhoff-Love plate and shell problems were studied in [27]. In [28–30] IGA-C was extended to geometrically nonlinear three-dimensional shear-deformable beams. Nonlinear planar Kirchhoff rods were formulated in [31]. In linear dynamics, an explicit IGA-C formulation was introduced in [2] and more recently an explicit higher-order space- and time-accurate method for elastodynamics was proposed in [32]. IGA-C methods for the nonlinear dynamics of geometrically exact beams, to our best knowledge, have been investigated so far only in [33] through an implicit quaternion-based formulation and in [34] through an explicit formulation based on the spatial incremental rotation vector.

In the present paper we propose an implicit scheme based on a full material description of the rotational unknowns. In a three-dimensional Timoshenko beam model, the (finite) rotation of each beam cross section is described by a time-depending orthogonal operator belonging to the non-commutative Lie group SO(3). On SO(3) rotation updates, namely transformations of SO(3) onto itself, are consistently performed by the composition of an incremental rotation with the current rotation. Such an operation, called translation, is non-additive and non-commutative. The latter attribute leads to a substantial difference between right translation (spatial description of the motion) and left translation (material description of the motion) on SO(3) [35–37]. Apart from the implicitness of the method, the fundamental difference with respect to our previous formulations [28, 30, 34] lies in that incremental rotations are now considered in the material setting, therefore rotation updates are performed via left translations. This change, necessary for an optimal combination with the SO(3)-extended version of the classical Newmark scheme originally proposed in [36], requires a new derivation of the linearized equations and new formulas for the update procedure. These two central issues are discussed in detail in the present paper.

In the standard FEA framework, after the seminal papers by Simo & Vu-Quoc [36] and Cardona & Geradin [38], several time integration schemes and nonlinear beam formulations have been proposed and discussed over the years [33, 37, 39–53]. Our choice of combining the SO(3) Newmark scheme with a kinematic model based on the material incremental rotation vector is made to endow the formulation with the following attributes: (i) high stability; (ii) full geometric consistency, namely the main operations of linearization, variables initialization and kinematic update are made consistently with the geometric structure of the configuration manifold; (iii) high efficiency, since rotational unknowns are represented by a minimum number of variables due to the use of the rotation-vector parameterization. Moreover, the time stepping algorithm is used in a full material framework. This is an improvement with respect to [36], where the primary rotational unknowns are expressed in the spatial form, while the time stepping algorithm is set in the material form. Thus, we avoid the repetitive and time-consuming pull-back and push-forward operations between the material and spatial manifolds; (iv) absence of singularities, since incremental rotations are always small.

The outline of the paper is as follows: in Section 2 we briefly review the three-dimensional shear-deformable beam kinematics with a focus on the construction of the material tangent space. In Section 3 the material strong form of the governing equations is presented in terms of kinematic variables only. Strain measures and the constitutive law are also briefly recalled. In Section 4 the main features of the Newmark time stepping scheme are discussed. Section 5, complemented with Appendix A, addresses the discretization of the governing equations and their consistent linearization. In Section 6 we describe the solution procedure focusing on the variables initialization and update formulas. In Section 7 we apply the proposed formulation to solve problems involving very large displacements and rotations with different boundary conditions. Finally, in Section 8, we draw the main conclusions of our work.

2. The configuration manifold and its (material) tangent space

In this section we briefly recall the geometric structure underlying the kinematics of the Timoshenko beam model.

The motion of any material particle $\boldsymbol{p} \in \mathcal{B}$ of a shear-deformable beam is expressed as $\boldsymbol{\varphi}(t, \boldsymbol{p}) = \boldsymbol{c}(t, \boldsymbol{q}) + \mathbf{R}(t, \boldsymbol{q})(\boldsymbol{p} - \boldsymbol{q})$ where t is the time, $\boldsymbol{q}$ is the material position of the centroid of the beam cross section containing point $\boldsymbol{p}$. $\mathcal{S} \subset \mathcal{B}$ is the centroid line, namely a one-dimensional space containing the centroids of all cross sections of the beam. On $\mathcal{S}$ we define a coordinate system $s : \mathcal{S} \rightarrow [0, L] \subset \mathrm{I\!R}$, where L is the length of the beam centroid line in the initial configuration. The configuration manifold is the set

$$\mathcal{C} = \left\{ (\boldsymbol{c}, \mathbf{R}) \,|\, \boldsymbol{c} : \boldsymbol{T} \times \mathcal{S} \rightarrow \mathrm{I\!R}^3 \,, \mathbf{R} : \boldsymbol{T} \times \mathcal{S} \rightarrow \mathrm{SO}(3) \right\} \,, \tag{1}$$

where $\boldsymbol{c}(t, \boldsymbol{q})$ is the spatial location of the center of mass of the beam cross section at time t and point $\boldsymbol{q} \in \mathcal{S}$, and $\mathbf{R}(t, \boldsymbol{q})$ is the rigid rotation of the same cross section at the same time. $\boldsymbol{T} = [0, T] \subset \mathrm{I\!R}$ denotes the time domain.

As opposed to our previous formulations [28, 30, 34], where the spatial formulation was used, here we need to introduce the material form of the tangent space to the configuration manifold at point $(\boldsymbol{c}, \mathbf{R}) \in \mathcal{C}$. The tangent space is denoted by $T_{(\boldsymbol{c},\mathbf{R})}\mathcal{C} = T_{\boldsymbol{c}}\mathrm{I\!R}^3 \times T_{\mathbf{R}}\,\mathrm{SO}(3)$, where $T_{\boldsymbol{c}}\mathrm{I\!R}^3$, the tangent space to $\mathrm{I\!R}^3$ at $\boldsymbol{c}$, is simply $\mathrm{I\!R}^3$, namely the set of vectors $\boldsymbol{\eta}$

applied in $\boldsymbol{c}$; whereas the (material) tangent space to SO(3) at $\mathbf{R}$ is given by $T_{\mathbf{R}}\,\mathrm{SO}(3) = \left\{\mathbf{R}\widetilde{\boldsymbol{\Theta}} \,|\, \widetilde{\boldsymbol{\Theta}} \in \mathrm{so}(3)\,, \mathbf{R} \in \mathrm{SO}(3)\right\}$. The construction of the material tangent space is made similarly to the spatial case [28] with the difference that the incremented rotation $\mathbf{R}_\varepsilon$ is obtained through left translation instead of right translation [35–37]. Namely, the (material) tangent space at $(\boldsymbol{c}, \mathbf{R})$ is obtained by $(d\boldsymbol{\gamma}/d\varepsilon)_{\varepsilon=0}$ where $\varepsilon \mapsto \boldsymbol{\gamma}(\varepsilon) = (\boldsymbol{c}_\varepsilon, \mathbf{R}_\varepsilon)$, with $\varepsilon \in \mathrm{I\!R}$, is a curve on $\mathcal{C}$ defined by $\boldsymbol{c}_\varepsilon = \boldsymbol{c} + \varepsilon\boldsymbol{\eta}$ (standard translation on $\mathrm{I\!R}^3$) and $\mathbf{R}_\varepsilon = \mathbf{R}\exp(\varepsilon\widetilde{\boldsymbol{\Theta}})$ (left translation on SO(3)), such that $\boldsymbol{\gamma}(0) = (\boldsymbol{c}, \mathbf{R})$. From the kinematic point of view, $\boldsymbol{\eta} \in \mathrm{I\!R}^3$ represents an incremental displacement superimposed to the current configuration of the centroid line $\boldsymbol{c}$; whereas $\widetilde{\boldsymbol{\Theta}}$, such that $\mathbf{R}\widetilde{\boldsymbol{\Theta}} \in T_{\mathbf{R}}\,\mathrm{SO}(3)$, represents an incremental rotation superimposed to the rotation $\mathbf{R}$. Note that in the construction of the curve $\boldsymbol{\gamma}$ we used the exponential map $\exp : \mathrm{so}(3) \to \mathrm{SO}(3)$ which maps the line $\varepsilon\widetilde{\boldsymbol{\Theta}}$ at so(3) onto the one parameter subgroup $\exp(\varepsilon\widetilde{\boldsymbol{\Theta}}) \in \mathrm{SO}(3)$ [35, p. 160]. This means that $\exp(\varepsilon\widetilde{\boldsymbol{\Theta}})$ is a rotation occurring around the fixed direction $\boldsymbol{\Theta} = \mathrm{axial}(\widetilde{\boldsymbol{\Theta}})$[1]. A fundamental aspect the present formulation relies on is that for SO(3) the exponential map is expressed by an exact (Rodrigues) formula [54–57].

For a more detailed discussion on the construction of tangent spaces to SO(3) reference is made to [36–38, 42, 44].

3. Balance equations in local form

We start this section by recalling the strong form of the balance equations using the material description. Since in this paper we develop a primal formulation, the equations are expressed in terms of kinematic quantities only. For this reason, we shortly review also the strain measures and the constitutive law.

The strong form of the balance equations [58] can be written in the material form as

[1] With the symbol $\sim$ we denote elements of so(3), that is the set of 3×3 skew-symmetric matrices that, in this context, represent infinitesimal incremental rotations. Furthermore, for any skew-symmetric matrix $\widetilde{\boldsymbol{a}} \in \mathrm{so}(3)$, $\boldsymbol{a} = \mathrm{axial}(\widetilde{\boldsymbol{a}})$ indicates the axial vector of $\widetilde{\boldsymbol{a}}$ such that $\widetilde{\boldsymbol{a}}\boldsymbol{h} = \boldsymbol{a} \times \boldsymbol{h}$, for any $\boldsymbol{h} \in \mathrm{I\!R}^3$.

follows

$$\mu \mathbf{R}^{\mathsf{T}} \boldsymbol{a} = \widetilde{\boldsymbol{K}} \mathbb{C}_N \boldsymbol{\Gamma}_N + \mathbb{C}_N \boldsymbol{\Gamma}_{N,s} + \mathbf{R}^{\mathsf{T}} \bar{\boldsymbol{n}} \,, \tag{2}$$

$$\boldsymbol{J} \boldsymbol{A} + \widetilde{\boldsymbol{W}} \boldsymbol{J} \boldsymbol{W} = \widetilde{\boldsymbol{K}} \mathbb{C}_M \boldsymbol{K}_M + \mathbb{C}_M \boldsymbol{K}_{M,s} + \mathbf{R}^{\mathsf{T}} \boldsymbol{c}_{,s} \times \mathbb{C}_N \boldsymbol{\Gamma}_N + \mathbf{R}^{\mathsf{T}} \bar{\boldsymbol{m}} \,, \tag{3}$$

valid for any $s \in (0, L)$ and $t \in (0, T]$. In the above equations μ is the mass per unit length of the beam; $\boldsymbol{a}$ is the spatial acceleration vector of the cross section centroid; $\widetilde{\boldsymbol{K}} = \mathbf{R}^{\mathsf{T}} \mathbf{R}_{,s}$ is the beam curvature (skew-symmetric tensor) in the material form; $\boldsymbol{\Gamma}_N$ and $\boldsymbol{K}_M$ are the strain measure vectors in the material form (better detailed later); $\bar{\boldsymbol{n}}$ and $\bar{\boldsymbol{m}}$ are the distributed external forces and moments per unit length in spatial form; $\boldsymbol{J}$ is the material (time-independent) inertia tensor; $\widetilde{\boldsymbol{W}} = \mathbf{R}^{\mathsf{T}} \dot{\mathbf{R}}$ is the material skew-symmetric angular velocity tensor and $\boldsymbol{W} = \mathrm{axial}(\widetilde{\boldsymbol{W}})$ its axial vector; $\boldsymbol{A} = \dot{\boldsymbol{W}}$ is the material angular acceleration vector; $\mathbb{C}_N = \mathrm{diag}(GA_1, EA, GA_3)$ and $\mathbb{C}_M = \mathrm{diag}(EJ_1, GJ, EJ_3)$, where GA_1 and GA_3 are the shear stiffnesses along the cross section principal axes, EA is the axial stiffness, GJ is the torsional stiffness, and EJ_1 and EJ_3 are the principal bending stiffnesses. Partial derivatives with respect to the coordinate $s : \mathcal{S} \to [0, L] \subset \mathbb{R}$ are indicated with $()_{,s}$, whereas $\dot{()}$ indicates the derivative with respect to time.

Boundary and initial conditions are given as follows

$$\boldsymbol{\eta} = \bar{\boldsymbol{\eta}}_c \quad \text{or} \quad \boldsymbol{N} = \mathbf{R}^{\mathsf{T}} \bar{\boldsymbol{n}}_c \quad \text{with} \quad s = \{0, L\}\,, t \in [0, T]\,, \tag{4}$$

$$\boldsymbol{\Theta} = \bar{\boldsymbol{\Theta}}_c \quad \text{or} \quad \boldsymbol{M} = \mathbf{R}^{\mathsf{T}} \bar{\boldsymbol{m}}_c \quad \text{with} \quad s = \{0, L\}\,, t \in [0, T]\,, \tag{5}$$

$$\boldsymbol{v} = \boldsymbol{v}_0 \quad \text{with} \quad s \in (0, L) \quad \text{and} \quad t = 0\,, \tag{6}$$

$$\boldsymbol{W} = \boldsymbol{W}_0 \quad \text{with} \quad s \in (0, L) \quad \text{and} \quad t = 0\,, \tag{7}$$

where $\boldsymbol{N}$ and $\boldsymbol{M}$ are the material internal forces and moments, respectively; $\bar{\boldsymbol{n}}_c$ and $\bar{\boldsymbol{m}}_c$ are the external concentrated forces and moments applied to any of the beam ends in the current configuration; $\boldsymbol{v}$ is the spatial velocity vector of the cross section centroid; $\bar{\boldsymbol{\eta}}_c$ and $\bar{\boldsymbol{\Theta}}_c$ are the prescribed displacement (spatial) and rotation (material) vectors at any of the beam ends.

We recall that the deformation measures in the material form are given by [58–60]

$$\boldsymbol{\Gamma}_N = \boldsymbol{\Gamma} - \boldsymbol{\Gamma}_0 = \mathbf{R}^{\mathsf{T}} \boldsymbol{c}_{,s} - \mathbf{R}_0^{\mathsf{T}} \boldsymbol{c}_{0,s} \quad \text{and} \quad \boldsymbol{K}_M = \mathrm{axial}(\widetilde{\boldsymbol{K}} - \widetilde{\boldsymbol{K}}_0) = \boldsymbol{K} - \boldsymbol{K}_0 \,, \tag{8}$$

where $\mathbf{\Gamma} = \mathbf{R}^\mathsf{T}\boldsymbol{c}_{,s} - [0\,1\,0]^\mathsf{T}$ and $\mathbf{\Gamma}_0 = \mathbf{R}_0^\mathsf{T}\boldsymbol{c}_{0,s} - [0\,1\,0]^\mathsf{T}$. $\mathbf{\Gamma}_N$ describes the axial and shear strains, whereas $\boldsymbol{K}_M$ describes the bending and torsional strains; $\widetilde{\boldsymbol{K}}_0 = \mathbf{R}_0^\mathsf{T}\mathbf{R}_{0,s}$ is the beam initial curvature (skew-symmetric tensor) in the material form; $\boldsymbol{c}_0$ represents the centroid line in the initial configuration; $\mathbf{R}_0 \in \mathrm{SO}(3)$ is the rotation operator that expresses the rotation of the beam cross section in the initial configuration [59, 60].

Under the assumption of a Saint Venant-Kirchhoff constitutive model, the material internal forces and moments are linearly related to the material strain measures as follows [38, 44, 61]

$$\boldsymbol{N} = \mathbb{C}_N\mathbf{\Gamma}_N \quad \text{and} \quad \boldsymbol{M} = \mathbb{C}_M\boldsymbol{K}_M\,. \tag{9}$$

4. Implicit time stepping algorithm

Before addressing the core of the formulation, in this section we review the Newmark time integration scheme extended to the rotation group SO(3) [36] and focus on some preparatory (but fundamental for the computational formulation) geometric aspects related to the use of different tangent spaces to SO(3).

4.1. The Newmark scheme

The material form of the Newmark algorithm for SO(3) [36] is given as follows

$$\mathbf{R}^{n+1} = \mathbf{R}^n \exp(\widetilde{\boldsymbol{\Theta}}^n)\,, \tag{10}$$

$$\boldsymbol{\Theta}^n = h\boldsymbol{W}^n + h^2\left[\left(\frac{1}{2} - \beta\right)\boldsymbol{A}^n + \beta\boldsymbol{A}^{n+1}\right]\,, \tag{11}$$

$$\boldsymbol{W}^{n+1} = \boldsymbol{W}^n + h\left[(1-\gamma)\,\boldsymbol{A}^n + \gamma\boldsymbol{A}^{n+1}\right]\,. \tag{12}$$

The superscript $n = 0, 1, \ldots$ is used to denote any temporal discrete and approximate quantity at time $t^n = nh$, where h is the time step size. $\beta \in [0, \frac{1}{2}]$ and $\gamma \in [0, 1]$ are the standard Newmark parameters. It is convenient for the developments in the next sections to express angular acceleration and velocity at time t^{n+1} in terms of quantities at t^n. By exploiting Eqs. (11) and (12) we have

$$\boldsymbol{A}^{n+1} = \frac{1}{\beta h^2}\,\boldsymbol{\Theta}^n - \boldsymbol{A}_*^n\,, \tag{13}$$

$$\boldsymbol{W}^{n+1} = \frac{\gamma}{\beta h}\,\boldsymbol{\Theta}^n + \boldsymbol{W}_*^n\,, \tag{14}$$

where we have set

$$\boldsymbol{A}_*^n = \frac{1}{h\beta}\,\boldsymbol{W}^n + (\frac{1}{2\beta} - 1)\boldsymbol{A}^n\,, \tag{15}$$

$$\boldsymbol{W}_*^n = (1 - \frac{\gamma}{\beta})\boldsymbol{W}^n + (1 - \frac{\gamma}{2\beta})h\boldsymbol{A}^n\,. \tag{16}$$

The algorithm used to integrate the motion of the beam centroid line is the standard Newmark for nonlinear dynamics, which, for the sake of completeness, is reported in the following

$$\boldsymbol{c}^{n+1} = \boldsymbol{c}^n + \boldsymbol{\eta}^n\,, \tag{17}$$

$$\boldsymbol{\eta}^n = h\boldsymbol{v}^n + h^2\left[\left(\frac{1}{2} - \beta\right)\boldsymbol{a}^n + \beta\boldsymbol{a}^{n+1}\right]\,, \tag{18}$$

$$\boldsymbol{v}^{n+1} = \boldsymbol{v}^n + h\left[(1-\gamma)\,\boldsymbol{v}^n + \gamma\boldsymbol{a}^{n+1}\right]\,. \tag{19}$$

As done for the rotational quantities, using Eqs. (18) and (19), angular acceleration and velocity at time t^{n+1} can be expressed as follows

$$\boldsymbol{a}^{n+1} = \frac{1}{\beta h^2}\,\boldsymbol{\eta}^n - \boldsymbol{a}_*^n\,, \tag{20}$$

$$\boldsymbol{v}^{n+1} = \frac{\gamma}{\beta h}\,\boldsymbol{\eta}^n + \boldsymbol{v}_*^n\,, \tag{21}$$

where we have set

$$\boldsymbol{a}_*^n = \frac{1}{h\beta}\,\boldsymbol{v}^n + (\frac{1}{2\beta} - 1)\boldsymbol{a}^n\,, \tag{22}$$

$$\boldsymbol{v}_*^n = (1 - \frac{\gamma}{\beta})\boldsymbol{v}^n + (1 - \frac{\gamma}{2\beta})h\boldsymbol{a}^n\,. \tag{23}$$

4.2. Relation between different tangent spaces to SO(3)

The numerical formulation we employ crucially relies on the correct identification of the tangent space the incremental rotations belong to [36, 37]. Roughly speaking, the tangent space is a geometric structure which permits to approximate locally the nonlinear manifold (SO(3) in our case) with a vector space ($\mathbb{R}^3$ in our case) where standard (additive and commutative) operations can be performed. The local nature of the tangent space represents the main complexity behind the numerical schemes involving finite rotations.

Starting from Eq. (10), an incremented rotation from $\mathbf{R}^{n+1}$ can be obtained in two different ways, in both cases by using left (material) translation, as follows

$$\mathbf{R}_{\varepsilon}^{n+1} = \mathbf{R}^{n+1} \exp(\varepsilon\delta\widetilde{\boldsymbol{\Theta}}^{n+1}) \,, \tag{24}$$

$$\mathbf{R}_{\varepsilon}^{n+1} = \mathbf{R}^{n} \exp(\widetilde{\boldsymbol{\Theta}}^{n} + \varepsilon\delta\widetilde{\boldsymbol{\Theta}}^{n}) \,. \tag{25}$$

Note that $\delta\widetilde{\boldsymbol{\Theta}}^{n+1}$ and $\delta\widetilde{\boldsymbol{\Theta}}^{n}$ are both incremental rotations but they refer to two different tangent spaces, namely $\delta\widetilde{\boldsymbol{\Theta}}^{n+1} \in T_{\mathbf{R}^{n+1}}\,\mathrm{SO}(3)$, whereas $\delta\widetilde{\boldsymbol{\Theta}}^{n} \in T_{\mathbf{R}^{n}}\,\mathrm{SO}(3)$. By exploiting Eq. (10) and the orthogonality property of the rotation operators, the two above equations lead to

$$\exp(\widetilde{\boldsymbol{\Theta}}^{n}) \exp(\varepsilon\delta\widetilde{\boldsymbol{\Theta}}^{n+1}) = \exp(\widetilde{\boldsymbol{\Theta}}^{n} + \varepsilon\delta\widetilde{\boldsymbol{\Theta}}^{n}) \,. \tag{26}$$

As demonstrated in [38], the above equation provides the relation between the incremental rotations belonging to two different tangent spaces. Namely, there exists a linear invertible mapping $\mathbf{T}(\boldsymbol{\Theta}^n) : T_{\mathbf{R}^{n}}\,\mathrm{SO}(3) \rightarrow T_{\mathbf{R}^{n+1}}\,\mathrm{SO}(3)$ such that[2]

$$\delta\boldsymbol{\Theta}^{n+1} = \mathbf{T}(\boldsymbol{\Theta}^n)\delta\boldsymbol{\Theta}^{n} \quad \text{and} \quad \delta\boldsymbol{\Theta}^{n} = \mathbf{T}^{-1}(\boldsymbol{\Theta}^n)\delta\boldsymbol{\Theta}^{n+1} \,. \tag{27}$$

Given the fundamental role of $\mathbf{T}^{-1}(\boldsymbol{\Theta}^n)$, as it will appear clear in the next section, we report its explicit expression leaving the details of the derivation in [38, 62]

$$\mathbf{T}^{-1}(\boldsymbol{\Theta}^n) = \mathbf{e}^n \otimes \mathbf{e}^n + \frac{||\boldsymbol{\Theta}^n||/2}{\tan(||\boldsymbol{\Theta}^n||/2)} \left(\mathbf{id} - \mathbf{e}^n \otimes \mathbf{e}^n\right) + \frac{1}{2}\,\widetilde{\boldsymbol{\Theta}}^{n} \,, \tag{28}$$

where $\mathbf{e}^n = \boldsymbol{\Theta}^n/||\boldsymbol{\Theta}^n||$.

As regards the translational motion of the cross section centroid, the mapping $\mathbf{T}$ turns out to be the identity map, namely $\delta\boldsymbol{\eta}^{n+1}$ and $\delta\boldsymbol{\eta}^{n}$ coincide.

5. Discretization of the governing equations and consistent linearization

In this section we first introduce the time discretized version of the governing equations. Then we proceed with the consistent linearization of the equations and finally we introduce the spatial discretization. Importantly, we remark that, unlike in [36] where the problem

[2] An abuse of notation is made here since the operator $\mathbf{T}(\boldsymbol{\Theta}^n)$ actually maps axial vectors and not the associated skew-symmetric matrices.

is solved in the spatial setting and the time integration is performed in the material frame, here we propose a procedure which is fully carried out in the material setting, resulting in an increased efficiency since the numerous pull-backs and push-forwards between the two settings are avoided.

5.1. Time-discretized governing equations

The balance equations (2) and (3) together with the Neumann boundary conditions Eqs. (4) and (5) must be satisfied at each time instant. We write the equations at t^{n+1} as follows

$$-\mu \mathbf{R}^{\mathsf{T}n+1}\boldsymbol{a}^{n+1} + \widetilde{\boldsymbol{K}}^{n+1}\mathbb{C}_N\boldsymbol{\Gamma}_N^{n+1} + \mathbb{C}_N\boldsymbol{\Gamma}_{N,s}^{n+1} + \mathbf{R}^{\mathsf{T}n+1}\bar{\boldsymbol{n}}^{n+1} = \mathbf{0}\,, \tag{29}$$

$$\begin{aligned} -(\boldsymbol{J}\boldsymbol{A}^{n+1} + \widetilde{\boldsymbol{W}}^{n+1}\boldsymbol{J}\boldsymbol{W}^{n+1}) + \widetilde{\boldsymbol{K}}^{n+1}\mathbb{C}_M\boldsymbol{K}_M^{n+1} + \\ \mathbb{C}_M\boldsymbol{K}_{M,s}^{n+1} + \mathbf{R}^{\mathsf{T}n+1}\boldsymbol{c}_{,s}^{n+1}\times\mathbb{C}_N\boldsymbol{\Gamma}_N^{n+1} + \mathbf{R}^{\mathsf{T}n+1}\bar{\boldsymbol{m}}^{n+1} = \mathbf{0}\,, \end{aligned} \tag{30}$$

$$\mathbb{C}_N\boldsymbol{\Gamma}_N^{n+1} - \mathbf{R}^{\mathsf{T}n+1}\bar{\boldsymbol{n}}_c^{n+1} = \mathbf{0}\,, \tag{31}$$

$$\mathbb{C}_M\boldsymbol{K}_M^{n+1} - \mathbf{R}^{\mathsf{T}n+1}\bar{\boldsymbol{m}}_c^{n+1} = \mathbf{0}\,. \tag{32}$$

5.2. Linearization of the time-discretized governing equations

Linearizations are performed making use of the directional derivatives reported in Appendix A. With the symbol $\hat{(\cdot)}$ we denote any quantity evaluated at the configuration t^{n+1} around which the linearization takes place. We start with the linearization of the translational equations and then proceed with the rotational equations. For the sake of clarity, we proceed systematically term by term.

5.2.1. Translational equations

The linearization of the inertia term of Eq. (29) leads to

$$\begin{aligned} L[\mu\mathbf{R}^{\mathsf{T}n+1}\boldsymbol{a}^{n+1}] = \mu\hat{\mathbf{R}}^{\mathsf{T}n+1}\hat{\boldsymbol{a}}^{n+1} + \mu\frac{d}{d\varepsilon}\left(\mathbf{R}_{\varepsilon}^{\mathsf{T}n+1}\boldsymbol{a}_{\varepsilon}^{n+1}\right)_{\varepsilon=0} = \\ \mu\hat{\mathbf{R}}^{\mathsf{T}n+1}\hat{\boldsymbol{a}}^{n+1} + \mu\left(\widetilde{\hat{\mathbf{R}}^{\mathsf{T}n+1}\hat{\boldsymbol{a}}^{n+1}}\right)\delta\boldsymbol{\Theta}^{n+1} + \frac{\mu}{h^2\beta}\hat{\mathbf{R}}^{\mathsf{T}n+1}\delta\boldsymbol{\eta}^{n+1}\,. \end{aligned} \tag{33}$$

Note that to obtain the above result we used the directional derivative of the acceleration given as follows

$$\frac{d}{d\varepsilon}\left(\boldsymbol{a}_{\varepsilon}^{n+1}\right)_{\varepsilon=0} = \frac{\delta\boldsymbol{\eta}^{n+1}}{\beta h^2}\,, \tag{34}$$

where use of Eq. (20) has been made.

Linearization of the second term of Eq. (29) is made as follows

$$
\begin{gathered}
L[\widetilde{\boldsymbol{K}}^{n+1}\mathbb{C}_N\boldsymbol{\Gamma}_N^{n+1}] = \widetilde{\hat{\boldsymbol{K}}}^{n+1}\mathbb{C}_N\hat{\boldsymbol{\Gamma}}_N^{n+1} + \frac{d}{d\varepsilon}\left(\widetilde{\boldsymbol{K}}_{\varepsilon}^{n+1}\mathbb{C}_N\boldsymbol{\Gamma}_{N\varepsilon}^{n+1}\right)_{\varepsilon=0} = \\
\widetilde{\hat{\boldsymbol{K}}}^{n+1}\mathbb{C}_N\hat{\boldsymbol{\Gamma}}_N^{n+1} + \left[\widetilde{\hat{\boldsymbol{K}}}^{n+1}\mathbb{C}_N\left(\widetilde{\hat{\mathbf{R}}^{\mathsf{T}n+1}\hat{\boldsymbol{c}}_{,s}^{n+1}}\right) - \left(\widetilde{\mathbb{C}_N\hat{\boldsymbol{\Gamma}}_N^{n+1}}\right)\widetilde{\hat{\boldsymbol{K}}}^{n+1}\right]\delta\boldsymbol{\Theta}^{n+1} - \\
\left[\widetilde{\mathbb{C}_N\hat{\boldsymbol{\Gamma}}_N^{n+1}}\right]\delta\boldsymbol{\Theta}_{,s}^{n+1} + \left[\widetilde{\hat{\boldsymbol{K}}}^{n+1}\mathbb{C}_N\hat{\mathbf{R}}^{\mathsf{T}n+1}\right]\delta\boldsymbol{\eta}^{n+1}{}_{,s}\ , \qquad (35)
\end{gathered}
$$

where we have used Eqs. (A.7) and (A.13).

Linearization of the third term of Eq. (29) is made as follows

$$
\begin{gathered}
L[\mathbb{C}_N\boldsymbol{\Gamma}_{N,s}^{n+1}] = \mathbb{C}_N\hat{\boldsymbol{\Gamma}}_{N,s}^{n+1} + \frac{d}{d\varepsilon}\left(\mathbb{C}_N\boldsymbol{\Gamma}_{N\varepsilon,s}^{n+1}\right)_{\varepsilon=0} = \\
\mathbb{C}_N\hat{\boldsymbol{\Gamma}}_{N,s}^{n+1} + \mathbb{C}_N\left[\left(\widetilde{\hat{\mathbf{R}}^{\mathsf{T}n+1}\hat{\boldsymbol{c}}_{,ss}^{n+1}}\right) - \left(\widetilde{\hat{\boldsymbol{K}}}(\widetilde{\hat{\mathbf{R}}^{\mathsf{T}n+1}\hat{\boldsymbol{c}}_{,s}^{n+1}})\right)\right]\delta\boldsymbol{\Theta}^{n+1} + \mathbb{C}_N\left[\widetilde{\hat{\mathbf{R}}^{\mathsf{T}n+1}\hat{\boldsymbol{c}}_{,s}^{n+1}}\right]\delta\boldsymbol{\Theta}_{,s}^{n+1} - \\
\mathbb{C}_N\left[\widetilde{\hat{\boldsymbol{K}}}^{n+1}\hat{\mathbf{R}}^{\mathsf{T}n+1}\right]\delta\boldsymbol{\eta}_{,s}^{n+1} + \mathbb{C}_N\left[\hat{\mathbf{R}}^{\mathsf{T}n+1}\right]\delta\boldsymbol{\eta}_{,ss}^{n+1}\ , \qquad (36)
\end{gathered}
$$

where we have used Eq. (A.14).

Linearization of the fourth term of Eq. (29) is made as follows

$$
L[\mathbf{R}_{\varepsilon}^{\mathsf{T}n+1}\bar{\boldsymbol{n}}^{n+1}] = \hat{\mathbf{R}}^{\mathsf{T}n+1}\bar{\boldsymbol{n}}^{n+1} + \left[\widetilde{\hat{\mathbf{R}}^{\mathsf{T}n+1}\bar{\boldsymbol{n}}^{n+1}}\right]\delta\boldsymbol{\Theta}^{n+1}\ , \qquad (37)
$$

where Eq. (A.4) has been used.

Linearization of the first term of the boundary condition (31) is made as follows

$$
L[\mathbb{C}_N\boldsymbol{\Gamma}_N^{n+1}] = \mathbb{C}_N\hat{\boldsymbol{\Gamma}}_N^{n+1} + \frac{d}{d\varepsilon}\left(\mathbb{C}_N\hat{\boldsymbol{\Gamma}}_{N\varepsilon}^{n+1}\right)_{\varepsilon=0} = \qquad (38)
$$

$$
\mathbb{C}_N\hat{\boldsymbol{\Gamma}}_N^{n+1} + \mathbb{C}_N\left(\widetilde{\hat{\mathbf{R}}^{\mathsf{T}n+1}\hat{\boldsymbol{c}}_{,s}^{n+1}}\right)\delta\boldsymbol{\Theta}^{n+1} + \mathbb{C}_N\hat{\mathbf{R}}^{\mathsf{T}n+1}\delta\boldsymbol{\eta}_{,s}^{n+1}\ , \qquad (39)
$$

where Eq. (A.13) has been used.

Linearization of the last term of boundary condition (31) is made as follows

$$
L[\mathbf{R}^{\mathsf{T}n+1}\bar{\boldsymbol{n}}_c^{n+1}] = \hat{\mathbf{R}}^{\mathsf{T}n+1}\bar{\boldsymbol{n}}_c^{n+1} + \frac{d}{d\varepsilon}\left(\mathbf{R}_{\varepsilon}^{\mathsf{T}n+1}\bar{\boldsymbol{n}}_c^{n+1}\right)_{\varepsilon=0} = \qquad (40)
$$

$$
\hat{\mathbf{R}}^{\mathsf{T}n+1}\bar{\boldsymbol{n}}_c^{n+1} + \left(\widetilde{\hat{\mathbf{R}}^{\mathsf{T}n+1}\bar{\boldsymbol{n}}_c^{n+1}}\right)\delta\boldsymbol{\Theta}^{n+1}\ , \qquad (41)
$$

where Eq. (A.4) has been used.

5.2.2. Rotational equations

Linearization of the inertia term of Eq. (30) is given as follows

$$
\begin{aligned}
L[\boldsymbol{J}\boldsymbol{A}^{n+1} + \widetilde{\boldsymbol{W}}^{n+1}\boldsymbol{J}\boldsymbol{W}^{n+1}] &= \boldsymbol{J}\hat{\boldsymbol{A}}^{n+1} + \hat{\widetilde{\boldsymbol{W}}}^{n+1}\boldsymbol{J}\hat{\boldsymbol{W}}^{n+1} + \frac{d}{d\varepsilon}\left(\boldsymbol{J}\boldsymbol{A}_{\varepsilon}^{n+1} + \widetilde{\boldsymbol{W}}_{\varepsilon}^{n+1}\boldsymbol{J}\boldsymbol{W}_{\varepsilon}^{n+1}\right)_{\varepsilon=0} = \\
&\boldsymbol{J}\hat{\boldsymbol{A}}^{n+1} + \hat{\widetilde{\boldsymbol{W}}}^{n+1}\boldsymbol{J}\hat{\boldsymbol{W}}^{n+1} + \left[\frac{1}{\beta h^2}\boldsymbol{J} - \frac{\gamma}{\beta h}\left(\widetilde{\boldsymbol{J}\hat{\boldsymbol{W}}^{n+1}} - \hat{\widetilde{\boldsymbol{W}}}^{n+1}\boldsymbol{J}\right)\right]\mathbf{T}^{-1}(\hat{\boldsymbol{\Theta}}^{n})\delta\boldsymbol{\Theta}^{n+1}\,. \qquad (42)
\end{aligned}
$$

Note that to obtain the above results we used the directional derivative of the angular velocity and accelerations. We first note that

$$
\boldsymbol{A}_{\varepsilon}^{n+1} = \frac{\boldsymbol{\Theta}^{n} + \varepsilon\delta\boldsymbol{\Theta}^{n}}{\beta h^2} - \boldsymbol{A}_{*}^{n}\,, \qquad (43)
$$

$$
\boldsymbol{W}_{\varepsilon}^{n+1} = \frac{\gamma\left(\boldsymbol{\Theta}^{n} + \varepsilon\delta\boldsymbol{\Theta}^{n}\right)}{\beta h} + \boldsymbol{W}_{*}^{n}\,, \qquad (44)
$$

from which it follows that

$$
L[\boldsymbol{W}_{\varepsilon}^{n+1}] = \hat{\boldsymbol{W}}^{n+1} + \frac{\gamma}{\beta h}\,\delta\boldsymbol{\Theta}^{n} = \hat{\boldsymbol{W}}^{n+1} + \frac{\gamma}{\beta h}\,\mathbf{T}^{-1}(\hat{\boldsymbol{\Theta}}^{n})\delta\boldsymbol{\Theta}^{n+1}\,, \qquad (45)
$$

$$
L[\boldsymbol{A}_{\varepsilon}^{n+1}] = \hat{\boldsymbol{A}}^{n+1} + \frac{1}{\beta h^2}\,\delta\boldsymbol{\Theta}^{n} = \hat{\boldsymbol{A}}^{n+1} + \frac{1}{\beta h^2}\,\mathbf{T}^{-1}(\hat{\boldsymbol{\Theta}}^{n})\delta\boldsymbol{\Theta}^{n+1}\,, \qquad (46)
$$

where we have used Eq. (27).

Linearization of the second term of Eq. (30) is made as follows

$$
\begin{aligned}
L[\widetilde{\boldsymbol{K}}^{n+1}\mathbb{C}_M\boldsymbol{K}_M^{n+1}] &= \hat{\widetilde{\boldsymbol{K}}}^{n+1}\mathbb{C}_M\hat{\boldsymbol{K}}_M^{n+1} + \frac{d}{d\varepsilon}\left(\widetilde{\boldsymbol{K}}_{\varepsilon}^{n+1}\mathbb{C}_M\boldsymbol{K}_{M\varepsilon}^{n+1}\right)_{\varepsilon=0} = \\
&\hat{\widetilde{\boldsymbol{K}}}^{n+1}\mathbb{C}_M\hat{\boldsymbol{K}}_M^{n+1} + \left[\hat{\widetilde{\boldsymbol{K}}}^{n+1}\mathbb{C}_M\hat{\widetilde{\boldsymbol{K}}}^{n+1} - \left(\widetilde{\mathbb{C}_M\hat{\boldsymbol{K}}_M}\right)\hat{\widetilde{\boldsymbol{K}}}\right]\delta\boldsymbol{\Theta}^{n+1} + \\
&\left[\hat{\widetilde{\boldsymbol{K}}}^{n+1}\mathbb{C}_M - \left(\widetilde{\mathbb{C}_M\hat{\boldsymbol{K}}_M}\right)\right]\delta\boldsymbol{\Theta}_{,s}^{n+1}\,, \qquad (47)
\end{aligned}
$$

where we used Eqs. (A.7) and (A.8).

Linearization of the third term of Eq. (3) is given by

$$
\begin{aligned}
L[\mathbb{C}_M\boldsymbol{K}_{M,s}^{n+1}] &= \mathbb{C}_M\hat{\boldsymbol{K}}_{M,s}^{n+1} + \frac{d}{d\varepsilon}\left(\mathbb{C}_M\boldsymbol{K}_{M\varepsilon,s}^{n+1}\right)_{\varepsilon=0} = \\
&\mathbb{C}_M\hat{\boldsymbol{K}}_{M,s}^{n+1} + \mathbb{C}_M\hat{\widetilde{\boldsymbol{K}}}_{,s}^{n+1}\delta\boldsymbol{\Theta}^{n+1} + \mathbb{C}_M\hat{\widetilde{\boldsymbol{K}}}^{n+1}\delta\boldsymbol{\Theta}_{,s}^{n+1} + \mathbb{C}_M\delta\boldsymbol{\Theta}_{,ss}^{n+1}\,, \qquad (48)
\end{aligned}
$$

where we used Eq. (A.12).

Linearization of the fourth term of Eq. (30) is made as follows

$$L[\mathbf{R}^{\mathsf{T}n+1}\boldsymbol{c},_s^{n+1} \times \mathbb{C}_N \boldsymbol{\Gamma}_N^{n+1}] = \hat{\mathbf{R}}^{\mathsf{T}n+1}\hat{\boldsymbol{c}},_s^{n+1} \times \mathbb{C}_N \hat{\boldsymbol{\Gamma}}_N^{n+1} + \frac{d}{d\varepsilon}\left(\mathbf{R}_\varepsilon^{\mathsf{T}n+1}\boldsymbol{c}_{\varepsilon,s}^{n+1} \times \mathbb{C}_N \boldsymbol{\Gamma}_{N\varepsilon}^{n+1}\right)_{\varepsilon=0} =$$
$$\hat{\mathbf{R}}^{\mathsf{T}n+1}\hat{\boldsymbol{c}},_s^{n+1} \times \mathbb{C}_N \hat{\boldsymbol{\Gamma}}_N^{n+1} + \left[\left(\widetilde{\hat{\mathbf{R}}^{\mathsf{T}n+1}\hat{\boldsymbol{c}},_s^{n+1}}\right)\mathbb{C}_N - \left(\widetilde{\mathbb{C}_N \boldsymbol{\Gamma}_N^{n+1}}\right)\right]\left(\widetilde{\hat{\mathbf{R}}^{\mathsf{T}n+1}\hat{\boldsymbol{c}},_s^{n+1}}\right)\delta\boldsymbol{\Theta}^{n+1} +$$
$$\left[\left(\widetilde{\hat{\mathbf{R}}^{\mathsf{T}n+1}\hat{\boldsymbol{c}},_s^{n+1}}\right)\mathbb{C}_N - \left(\widetilde{\mathbb{C}_N \boldsymbol{\Gamma}_N^{n+1}}\right)\right]\hat{\mathbf{R}}^{\mathsf{T}n+1}\delta\boldsymbol{\eta},_s^{n+1}\ , \tag{49}$$

where use has been made of Eqs. (A.4), (A.1) and (A.13).

Linearization of the last term of Eq. (30) is made as follows

$$L[\mathbf{R}^{\mathsf{T}n+1}\bar{\boldsymbol{m}}^{n+1}] = \hat{\mathbf{R}}^{\mathsf{T}n+1}\bar{\boldsymbol{m}}^{n+1} + \frac{d}{d\varepsilon}\left(\mathbf{R}_\varepsilon^{\mathsf{T}n+1}\bar{\boldsymbol{m}}^{n+1}\right)_{\varepsilon=0} =$$
$$\hat{\mathbf{R}}^{\mathsf{T}n+1}\bar{\boldsymbol{m}}^{n+1} + \left(\widetilde{\hat{\mathbf{R}}^{\mathsf{T}n+1}\bar{\boldsymbol{m}}^{n+1}}\right)\delta\boldsymbol{\Theta}^{n+1}\,, \tag{50}$$

where use has been made of Eq. (A.4).

Linearization of the first term of boundary condition (32) is made as follows

$$L[\mathbb{C}_M \boldsymbol{K}_M^{n+1}] = \mathbb{C}_M \hat{\boldsymbol{K}}_M^{n+1} + \frac{d}{d\varepsilon}\left(\mathbb{C}_M \boldsymbol{K}_{M\varepsilon}^{n+1}\right)_{\varepsilon=0} = \tag{51}$$
$$\mathbb{C}_M \hat{\boldsymbol{K}}_M^{n+1} + \mathbb{C}_M \widetilde{\hat{\boldsymbol{K}}}^{n+1}\delta\boldsymbol{\Theta}^{n+1} + \mathbb{C}_M \delta\boldsymbol{\Theta},_s^{n+1}\ , \tag{52}$$

where we used Eq. (A.8).

Linearization of the last term of boundary condition (32) is made as follows

$$L[\mathbf{R}^{\mathsf{T}n+1}\bar{\boldsymbol{m}}_c^{n+1}] = \hat{\mathbf{R}}^{\mathsf{T}n+1}\bar{\boldsymbol{m}}_c^{n+1} + \frac{d}{d\varepsilon}\left(\mathbf{R}_\varepsilon^{\mathsf{T}n+1}\bar{\boldsymbol{m}}_c^{n+1}\right)_{\varepsilon=0} = \tag{53}$$
$$\hat{\mathbf{R}}^{\mathsf{T}n+1}\bar{\boldsymbol{m}}_c^{n+1} + \left(\widetilde{\hat{\mathbf{R}}^{\mathsf{T}n+1}\bar{\boldsymbol{m}}_c^{n+1}}\right)\delta\boldsymbol{\Theta}^{n+1}\,, \tag{54}$$

where we used Eq. (A.4).

5.3. Space discretization of the linearized equations

The linearized governing equations discussed above are written at time t^{n+1} but in space are still valid for any point $\boldsymbol{q} \in \mathcal{S}$. The linearized problem is turned into an algebraic system of equations first by discretizing the primary variables $\delta\boldsymbol{\Theta}^{n+1}$ and $\delta\boldsymbol{\eta}^{n+1}$ and then by collocating the time and space discretized equations in a set of points named collocation points. Space discretization is made using NURBS basis functions as follows

$$\boldsymbol{c}^{n+1}(u) = \sum_{j=0}^{\mathrm{n}} R_{j,p}(u)\check{\boldsymbol{p}}_j^{n+1} \quad \text{with} \quad u \in \mathcal{I}_u\,, \tag{55}$$

$$\delta\boldsymbol{\Theta}^{n+1}(u) = \sum_{j=0}^{\mathrm{n}} R_{j,p}(u)\delta\check{\boldsymbol{\Theta}}_j^{n+1} \quad \text{with} \quad u \in \mathcal{I}_u\,, \tag{56}$$

$$\delta\boldsymbol{\eta}^{n+1}(u) = \sum_{j=0}^{\mathrm{n}} R_{j,p}(u)\delta\check{\boldsymbol{\eta}}_j^{n+1} \quad \text{with} \quad u \in \mathcal{I}_u\,, \tag{57}$$

where $\mathcal{I}_u = [0, 1]$ is the normalized one-dimensional domain of the jth NURBS basis function $R_{j,p}$. $\check{\boldsymbol{p}}_j^{n+1}$ is the jth control point defining the centroid line; $\delta\check{\boldsymbol{\Theta}}_j^{n+1}$ and $\delta\check{\boldsymbol{\eta}}_j^{n+1}$ are the jth incremental control variables of the kinematic fields, which for $j = 0, \ldots, \mathrm{n}$, form the set of $2 \times 3 \times (\mathrm{n} + 1)$ unknowns of the algebraic system.

Recent studies proposed alternative choices for collocation points that can achieve improved convergence rates [18, 63–65]; however, in the present study we collocate at the standard Greville points [1].

6. Step by step description of the time integration scheme

At the time instant t^{n+1} the solution of the linearized problem must be searched for iteratively until convergence is achieved within a classical Newton-Raphson scheme. In this section we present the two fundamental steps that need to be accomplished: the initialization of the variables and the update procedure. Both operations must be performed in a geometrically consistent way.

Note that in the following we use the subscript i to denote the ith collocation point (of parametric coordinate u_i^c), whereas superscripts n, k are used to denote the time step and the iteration counter, respectively.

6.1. Initialization of variables at t^{n+1}

A correct initialization of the system matrix, namely the initialization of all $\hat{(\cdot)}$ quantities appearing in the linearized equations, has a crucial role in the reliability of the method. Assume that configuration $(\boldsymbol{c}_i^n, \mathbf{R}_i^n)$, velocities $\boldsymbol{W}_i^n, \boldsymbol{v}_i^n$, accelerations $\boldsymbol{A}_i^n, \boldsymbol{a}_i^n$, and the strain measures $\mathbf{\Gamma}^n_{Ni}$, $\boldsymbol{K}^n_{Mi}$ (and their derivatives) are known at t^n in each collocation point u^c_i with $i = 0, \ldots, \text{n}$.

First $\boldsymbol{\Theta}^n_i$ and $\boldsymbol{\eta}^n_i$ are initialized by using the predictors in Eqs. (11) and (18) as follows

$$\boldsymbol{\Theta}^{n,0}_i = h\boldsymbol{W}^n_i + h^2\left(\frac{1}{2} - \beta\right)\boldsymbol{A}^n_i\,, \tag{58}$$

$$\boldsymbol{\eta}^{n,0}_i = h\boldsymbol{v}^n_i + h^2\left(\frac{1}{2} - \beta\right)\boldsymbol{a}^n_i\,, \tag{59}$$

With Eqs. (58) and (59) at hand, all kinematic quantities can be initialized at time t^{n+1} as follows:

- The configuration is initialized as follows

$$\check{\boldsymbol{p}}^{n+1,0}_j = \check{\boldsymbol{p}}^n_j + \check{\boldsymbol{\eta}}^{n,0}_j\,, \tag{60}$$

$$\mathbf{R}^{n+1,0}_i = \mathbf{R}^n_i \exp(\widetilde{\boldsymbol{\Theta}}^{n,0}_i)\,, \tag{61}$$

  where incremental displacements $\check{\boldsymbol{\eta}}^{n,0}_j$ are obtained from the corresponding collocated quantities $\boldsymbol{\eta}^{n,0}_i$ given in Eq. (59).

- Accelerations and velocities are initialized by making use of Eqs. (13), (14), (20) and (21) as follows

$$\boldsymbol{A}^{n+1,0}_i = \frac{1}{\beta h^2}\,\boldsymbol{\Theta}^{n,0}_i - \boldsymbol{A}^n_{*i}\,, \tag{62}$$

$$\boldsymbol{W}^{n+1,0}_i = \frac{\gamma}{\beta h}\,\boldsymbol{\Theta}^{n,0}_i + \boldsymbol{W}^n_{*i}\,, \tag{63}$$

$$\boldsymbol{a}^{n+1,0}_i = \frac{1}{\beta h^2}\,\boldsymbol{\eta}^{n,0}_i - \boldsymbol{a}^n_{*i}\,, \tag{64}$$

$$\boldsymbol{v}^{n+1,0}_i = \frac{\gamma}{\beta h}\,\boldsymbol{\eta}^{n,0}_i + \boldsymbol{v}^n_{*i}\,. \tag{65}$$

- Curvature tensors. By recalling the definition of the material curvature tensor, which in the time discretized form reads $\widetilde{\boldsymbol{K}}^{n+1,0} = \mathbf{R}^{\mathsf{T}\,n+1,0}\mathbf{R}^{n+1,0}_{,s}$, and knowing that $\mathbf{R}^{n+1,0} = \mathbf{R}^n \exp(\widetilde{\boldsymbol{\Theta}}^{n,0})$, we obtain at the ith collocation point

$$\widetilde{\boldsymbol{K}}^{n+1,0}_i = \exp(-\widetilde{\boldsymbol{\Theta}}^{n,0}_i)\widetilde{\boldsymbol{K}}^n_i \exp(\widetilde{\boldsymbol{\Theta}}^{n,0}_i) + d\exp_{\widetilde{\boldsymbol{\Theta}}^{n,0}_i}(\widetilde{\boldsymbol{\Theta}}^{n,0}_{i,s})\,. \tag{66}$$

  In the above formula we made use of the rule $(\exp(\widetilde{\boldsymbol{\Theta}}(s))_{,s} = \exp(\widetilde{\boldsymbol{\Theta}})(d\exp_{\widetilde{\boldsymbol{\Theta}}})\widetilde{\boldsymbol{\Theta}}_{,s}$, where the operator $d\exp_{\widetilde{\boldsymbol{\Theta}}}$ is expressed by a series involving nested Lie bracket (see [28, Appendix B] and [66, p. 15] for further details).

In a similar way the initialization formula for the derivative of the material curvature tensor is obtained as follows

$$
\begin{aligned}
\widetilde{\boldsymbol{K}}_{i,s}^{n+1,0} = \exp(-\widetilde{\boldsymbol{\Theta}}_i^{n,0}) d\exp_{-\widetilde{\boldsymbol{\Theta}}_i^{n,0}}(-\widetilde{\boldsymbol{\Theta}}_{i,s}^{n,0})\widetilde{\boldsymbol{K}}_i^{n} \exp(\widetilde{\boldsymbol{\Theta}}_i^{n,0}) + \\
\exp(-\widetilde{\boldsymbol{\Theta}}_i^{n,0})\widetilde{\boldsymbol{K}}_{i,s}^{n} \exp(\widetilde{\boldsymbol{\Theta}}_i^{n,0}) + \\
\exp(-\widetilde{\boldsymbol{\Theta}}_i^{n,0})\widetilde{\boldsymbol{K}}_i^{n} \exp(\widetilde{\boldsymbol{\Theta}}_i^{n,0}) d\exp_{\widetilde{\boldsymbol{\Theta}}_i^{n,0}}(\widetilde{\boldsymbol{\Theta}}_{i,s}^{n,0}) + \\
\left(d\exp_{\widetilde{\boldsymbol{\Theta}}_i^{n,0}}(\widetilde{\boldsymbol{\Theta}}_{i,s}^{n,0})\right),_s \;. \qquad (67)
\end{aligned}
$$

The series expressing the operator $d\exp_{\widetilde{\boldsymbol{\Theta}}}$ permits also to compute the second derivative of the exponential map $(d\exp_{\widetilde{\boldsymbol{\Theta}}} \widetilde{\boldsymbol{\Theta}},_s),_s$ appearing in Eq. (67) keeping terms up to the desired order. The derivatives of the incremental rotation appearing in the above formulas are computed by using the discretization $\boldsymbol{\Theta}^{n,0} = \sum_{j=0}^{\mathrm{n}} R_{j,p}(u)\check{\boldsymbol{\Theta}}_j^{n,0}$, where the incremental rotations $\check{\boldsymbol{\Theta}}_j^{n,0}$ are obtained from the corresponding collocated quantities $\boldsymbol{\Theta}_i^{n,0}$ given in Eq. (58)[3].

- Strain measures defined in Eq. (8) and their derivatives are initialized using the above quantities as follows

$$\boldsymbol{\Gamma}_{Ni}^{n+1,0} = \boldsymbol{\Gamma}_i^{n+1,0} - \boldsymbol{\Gamma}_{0i} \qquad (68)$$

$$\boldsymbol{\Gamma}_{Ni,s}^{n+1,0} = \boldsymbol{\Gamma}_{i,s}^{n+1,0} - \boldsymbol{\Gamma}_{0i,s} \qquad (69)$$

$$\widetilde{\boldsymbol{K}}_{Mi}^{n+1,0} = \widetilde{\boldsymbol{K}}_i^{n+1,0} - \widetilde{\boldsymbol{K}}_{0i} \qquad (70)$$

$$\widetilde{\boldsymbol{K}}_{Mi,s}^{n+1,0} = \widetilde{\boldsymbol{K}}_{i,s}^{n+1,0} - \widetilde{\boldsymbol{K}}_{0i,s} \qquad (71)$$

where $\boldsymbol{\Gamma}_i^{n+1,0} = \mathbf{R}_i^{\mathsf{T}\,n+1,0}\boldsymbol{c}_{i,s}^{n+1,0} - [0\,1\,0]^{\mathsf{T}}$ and $\boldsymbol{\Gamma}_{i,s}^{n+1,0} = -\widetilde{\boldsymbol{K}}_i^{n+1,0}\mathbf{R}_i^{\mathsf{T}\,n+1,0}\boldsymbol{c}_{i,s}^{n+1,0} + \mathbf{R}_i^{\mathsf{T}\,n+1,0}\boldsymbol{c}_{i,ss}^{n+1,0}$. Derivatives of the centroid position are calculated by using the initialized control points given in Eq. (59) .

[3] First and second-order derivatives with respect to the physical coordinate $s \in [0, L]$ need to be calculated taking into account the change of parameterization required since NURBS basis functions are defined on the normalized domain $\mathcal{I}_u = [0, 1]$. Namely, for any quantity $\boldsymbol{g} : \mathcal{S} \to \mathbb{R}^3$, we have that $\boldsymbol{g},_s = \boldsymbol{g},_u / \jmath_0$ and $\boldsymbol{g},_{ss} = \boldsymbol{g},_{uu} / \jmath_0^2 - \boldsymbol{g},_u (\boldsymbol{c}_{0,u} \cdot \boldsymbol{c}_{0,uu})/\jmath_0^4$, where $\jmath_0 = ||\boldsymbol{c}_{0,u}||$ is the jacobian and $\cdot$ indicates the scalar product.

6.2. Update procedure

Once the initialization procedure described in the above section has been accomplished, the iteration procedure starts. Assume that at the kth iteration (with $k = 0, 1, 2 \ldots$) the configuration ($\boldsymbol{c}_i^{n+1,k}$, $\mathbf{R}_i^{\mathsf{T}\,n+1,k}$) and all other relevant kinematic variables are known. The solution of the system matrix provides control incremental rotation and displacement vectors $\delta\check{\boldsymbol{\Theta}}_j^{n+1,k}, \delta\check{\boldsymbol{\eta}}_j^{n+1,k}$. With a procedure similar to the one used in [28], but with the fundamental difference that here we employ the material incremental rotation vector, the geometrically consistent update procedure is performed as follows.

Control points are updated by exploiting the standard translation in $\mathbb{R}^3$

$$\check{\boldsymbol{p}}_j^{n+1,k+1} = \check{\boldsymbol{p}}_j^{n+1,k} + \delta\check{\boldsymbol{\eta}}_j^{n+1,k} , \tag{72}$$

from which we update the configuration of the centroid line

$$\boldsymbol{c}_i^{n+1,k+1} = \sum_{j=0}^{\mathrm{n}} R_{j,p}(u_i^c)\check{\boldsymbol{p}}_j^{n+1,k+1} . \tag{73}$$

For the rotation variables, we compute the incremental material rotation vector

$$\delta\boldsymbol{\Theta}_i^{n+1,k} = \sum_{j=0}^{\mathrm{n}} R_{j,p}(u_i^c)\delta\check{\boldsymbol{\Theta}}_j^{n+1,k} , \tag{74}$$

then the rotation operator is consistently updated as follows

$$\mathbf{R}_i^{n+1,k+1} = \mathbf{R}_i^{n+1,k} \exp(\delta\widetilde{\boldsymbol{\Theta}}_i^{n+1,k}) . \tag{75}$$

Update of the curvature tensor and its derivative is made through formulas similar to those used for their initialization (see Eqs. (66) and (67)). Namely we have

$$\widetilde{\boldsymbol{K}}_i^{n+1,k+1} = \exp(-\delta\widetilde{\boldsymbol{\Theta}}_i^{n+1,k})\widetilde{\boldsymbol{K}}_i^{n+1,k} \exp(\delta\widetilde{\boldsymbol{\Theta}}_i^{n+1,k}) + d\exp_{\widetilde{\boldsymbol{\Theta}}_i^{n+1,k}}(\delta\widetilde{\boldsymbol{\Theta}}_{i,s}^{n+1,k}) , \tag{76}$$

and

$$\begin{aligned} \widetilde{\boldsymbol{K}}_{i,s}^{n+1,k+1} = {} & \exp(-\delta\widetilde{\boldsymbol{\Theta}}_i^{n+1,k}) d\exp_{-\delta\widetilde{\boldsymbol{\Theta}}_i^{n+1,k}}(-\delta\widetilde{\boldsymbol{\Theta}}_{i,s}^{n+1,k})\widetilde{\boldsymbol{K}}_i^{n+1,k} \exp(\delta\widetilde{\boldsymbol{\Theta}}_i^{n+1,k}) + \\ & \exp(-\delta\widetilde{\boldsymbol{\Theta}}_i^{n+1,k})\widetilde{\boldsymbol{K}}_{i,s}^{n+1,k} \exp(\delta\widetilde{\boldsymbol{\Theta}}_i^{n+1,k}) + \\ & \exp(-\delta\widetilde{\boldsymbol{\Theta}}_i^{n+1,k})\widetilde{\boldsymbol{K}}_i^{n+1,k} \exp(\delta\widetilde{\boldsymbol{\Theta}}_i^{n+1,k}) d\exp_{\delta\widetilde{\boldsymbol{\Theta}}_i^{n+1,k}}(\delta\widetilde{\boldsymbol{\Theta}}_{i,s}^{n+1,k}) + \\ & \left(d\exp_{\delta\widetilde{\boldsymbol{\Theta}}_i^{n+1,k}}(\delta\widetilde{\boldsymbol{\Theta}}_{i,s}^{n+1,k})\right)_{,s} . \end{aligned} \tag{77}$$

The above updating formulas are obtained by following a very similar procedure used for Eqs. (66) and (67) with the difference that in this case $\widetilde{\boldsymbol{K}}^{n+1,k+1} = \mathbf{R}^{\mathsf{T}\,n+1,k+1}\mathbf{R}_{,s}^{n+1,k+1}$ where $\mathbf{R}^{n+1,k+1} = \mathbf{R}^{n+1,k}\exp(\delta\widetilde{\boldsymbol{\Theta}}^{n+1,k})$.

The updates of the strain measure vectors $\boldsymbol{K}_{Mi}^{n+1,k+1}$ and $\boldsymbol{\Gamma}_{Ni}^{n+1,k+1}$ and their derivatives are made straightforwardly by using the updated kinematic variables presented above.

Finally we need to update accelerations and velocities. Making use of Eqs. (13) and (14) expressed once in terms of $\boldsymbol{\Theta}^{n,k}$ and once in terms of $\boldsymbol{\Theta}^{n,k+1}$, see [36] for the details, we obtain the following update formulas

$$\boldsymbol{A}_i^{n+1,k+1} = \boldsymbol{A}_i^{n+1,k} + \frac{1}{\beta h^2}\left(\boldsymbol{\Theta}_i^{n,k+1} - \boldsymbol{\Theta}_i^{n,k}\right), \tag{78}$$

$$\boldsymbol{W}_i^{n+1,k+1} = \boldsymbol{W}_i^{n+1,k} + \frac{\gamma}{\beta h}\left(\boldsymbol{\Theta}_i^{n,k+1} - \boldsymbol{\Theta}_i^{n,k}\right), \tag{79}$$

where $\boldsymbol{\Theta}_i^{n,k}$ is known from the previous iteration, whereas we still have to compute $\boldsymbol{\Theta}_i^{n,k+1}$. To this end we recall that $\boldsymbol{\Theta}_i^{n,k+1}$ is such that

$$\mathbf{R}_i^{n+1,k+1} = \mathbf{R}_i^{n}\exp(\widetilde{\boldsymbol{\Theta}}^{n,k+1}), \tag{80}$$

from which we extract the incremental rotation vector by making use of the inverse of the exponential operator [36, 37, 67] as follows

$$\widetilde{\boldsymbol{\Theta}}_i^{n,k+1} = \exp^{-1}\left(\mathbf{R}_i^{\mathsf{T}\,n}\mathbf{R}_i^{n+1,k+1}\right), \tag{81}$$

where $\mathbf{R}_i^{\mathsf{T}\,n+1,k}$ is given by $\mathbf{R}_i^{n+1,k}\exp(\delta\widetilde{\boldsymbol{\Theta}}^{n+1,k})$.

In a similar way, but without the complexity related to SO(3), update formulas for linear acceleration and velocity are given by

$$\boldsymbol{a}_i^{n+1,k+1} = \boldsymbol{a}_i^{n+1,k} + \frac{1}{\beta h^2}\,\delta\boldsymbol{\eta}_i^{n+1,k}, \tag{82}$$

$$\boldsymbol{v}_i^{n+1,k+1} = \boldsymbol{v}_i^{n+1,k} + \frac{\gamma}{\beta h}\,\delta\boldsymbol{\eta}_i^{n+1,k}. \tag{83}$$

Once all kinematic variables are consistently updated $k+1 \rightarrow k$ and a new system matrix and residual vector can be defined. The algorithm proceeds until the L_2 norm of the incremental vector $[\delta\check{\boldsymbol{\Theta}}_j^{n+1,k}, \delta\check{\boldsymbol{\eta}}_j^{n+1,k}]^{\mathsf{T}}$ is reduced below a given tolerance; after that $n+1 \rightarrow n$ and a new time step starts with the initialization procedure discussed at the beginning of this section.

7. Numerical results and discussion

In this section we present the results of three numerical examples selected to test the capabilities of the proposed formulation in different conditions, including very fast dynamics with high-frequency vibrations, very large two- and three-dimensional deformations as well as different boundary conditions. In all cases we use $\beta = 0.25$ and $\gamma = 0.5$ to ensure second-order time-accuracy.

7.1. Cantilever beam

We begin with the case of the cantilever beam that we analyzed in [34] with an IGA-C explicit formulation. The test, originally proposed in [68], consists of a beam of length 1 m and with a square cross section with side 0.01 m. The Young's modulus is $E = 210 \times 10^9\,\mathrm{N/m^2}$, the Poisson's ratio is $\nu = 0.2$ and the material density is $\rho = 7800\,\mathrm{kg/m^3}$. With respect to a Cartesian reference system (x_1, x_2, x_3), initially the beam axis is placed along x_2 and the deformation occurs in the (x_2, x_3) plane due to a constant concentrated transversal tip force $\bar{n}_{c_3}$. In Figure 1 the time histories of the beam tip displacements are shown. Two load intensities: $\bar{n}_{c_3} = -10\,\mathrm{N}$ and $\bar{n}_{c_3} = -100\,\mathrm{N}$, the same as in [68] and [34], respectively, are considered. The loads are applied with constant intensity for a duration of 0.5 s through a step-function without any ramp. For both cases $p = 4$ and n = 20. An excellent agreement is found with [68] (for the small amplitude vibrations case) and with [34] for both small and large amplitude vibrations cases. The present implicit formulation appears particularly efficient since it is able to reproduce very fast nonlinear dynamics with impulsive loads (no load ramp functions are applied to any of the two load intensities) with a time step 500 times larger than the explicit formulation. Note that four iterations per time step are required in the Newton-Raphson algorithm with a tolerance on the L_2 norm of the incremental vector of 10^{-10}.

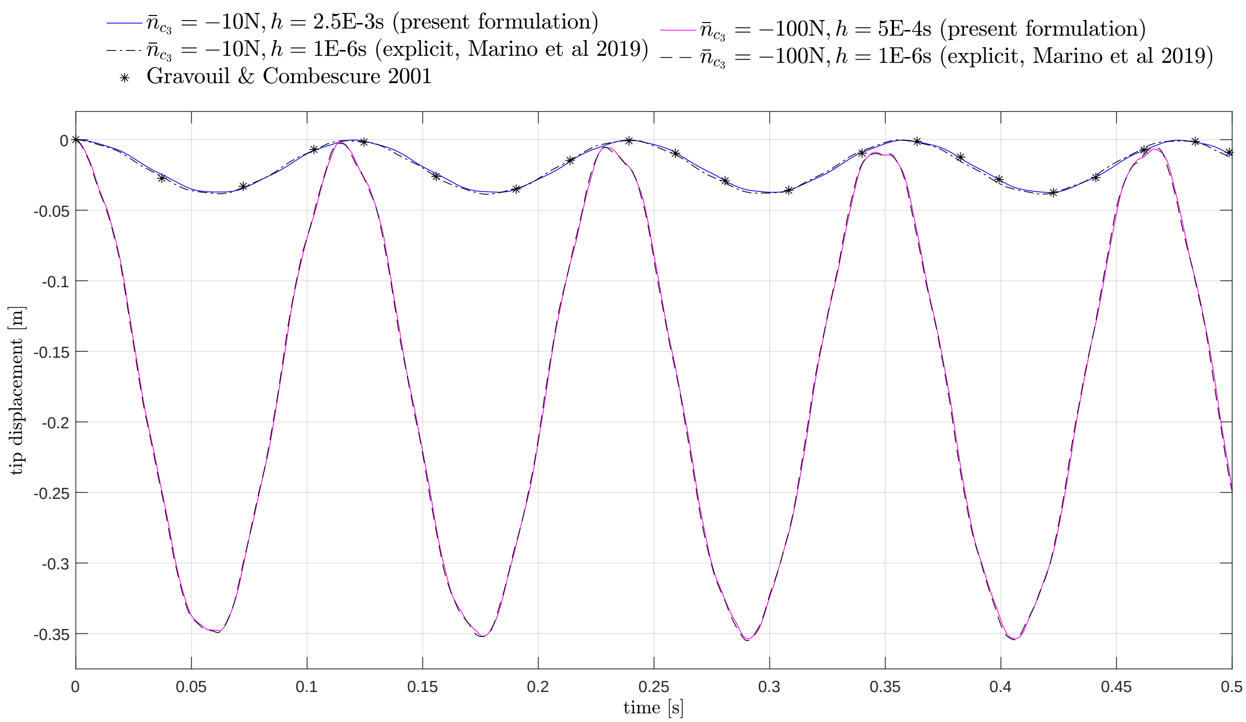

Figure 1: Tip displacement of a cantilever beam subjected to a tip transversal load F_3 with two different intensities. In both cases $p = 4$ and n = 20. Comparisons are made with results obtained in Marino et al 2019 [34] and Gravouil & Combescure 2001 [68].

7.2. Swinging flexible pendulum

Unlike in the previous numerical application, where a very stiff beam is considered, in this second example we study a highly flexible beam moving like a pendulum. The performance of the present formulation is analyzed through a direct comparison with the results obtained in [33, 46] and with our results obtained in [34] through an explicit formulation. The test consists of an initially straight beam of length 1 m with a circular cross section of diameter 0.01 m. The Young's modulus is $E = 5 \times 10^6\,\mathrm{N/m^2}$, the Poisson's ratio is $\nu = 0.5$ and the material density is $\rho = 1100\,\mathrm{kg/m^3}$. With respect to a Cartesian reference system (x_1, x_2, x_3), the beam, initially placed along x_2, is hinged at the end located at $(0, 0, 0)$ and is free at the other end. The motion occurs in the (x_2, x_3) plane under the effect of the gravity only acting along the x_3 direction. The distributed external force per unit length is $\bar{\boldsymbol{n}} = [0, 0, -0.8475]^\mathsf{T}$ N/m.

Figure 2 shows eleven snapshots taken from time 0 to 1 s with increments of 0.1 s. Results associated with different combinations of basis function degrees, number of collocation points and time step sizes are shown. Furthermore, considering the solution with $p = 6$, n $=$ 30, $h = 5 \times 10^{-3}$ s (see black line in the figure) as the most accurate one among the six analyses performed, some additional observations can be made. Up to approximately 0.5 s, the differences between all cases are almost indistinguishable. After that time, the results with $p = 4$ exhibit some loss of accuracy, while the results with $p = 6$ are always very accurate, also when using a coarser mesh (red line) or when doubling the time step size (green line), indicating that the error due to the space discretization dominates and can be easily (and efficiently) reduced by order elevation. In the IGA-C context, where efficiency is one of the major goals, such an attribute is highly desirable since order elevation is made almost at no additional computational cost.

The time history of the tip displacement is shown in Figure 3, where an excellent agreement with the results obtained in [33, 34, 46] is found.

7.3. Three-dimensional flying beam

The third numerical example has been chosen to assess the capabilities of the present formulation when very large and complex three-dimensional deformations occur. The test,

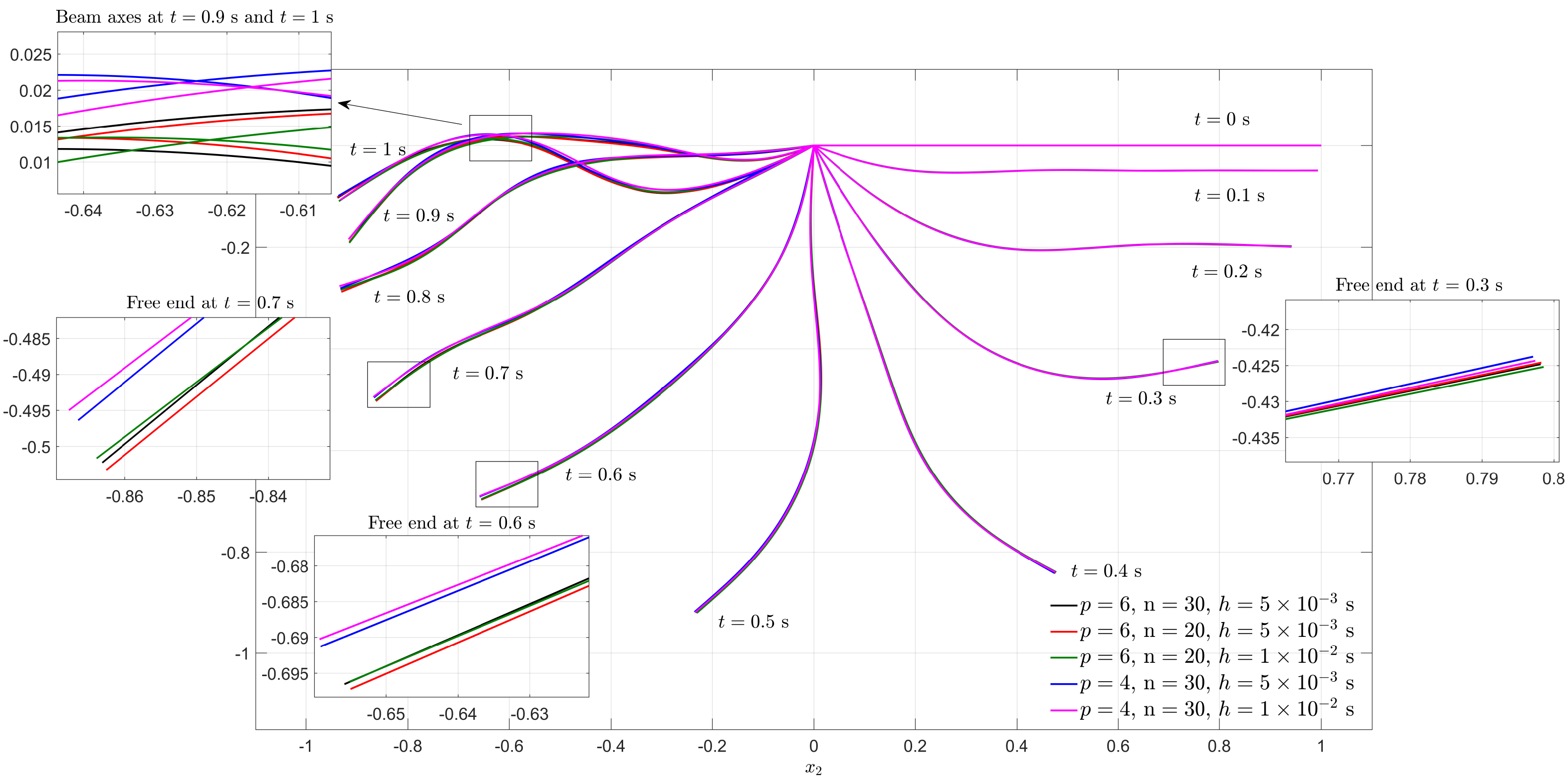

Figure 2: Snapshots of a swinging flexible pendulum from time 0 to 1 s with increments of 0.1 s for different basis function degrees, number of collocation points and time step spans.

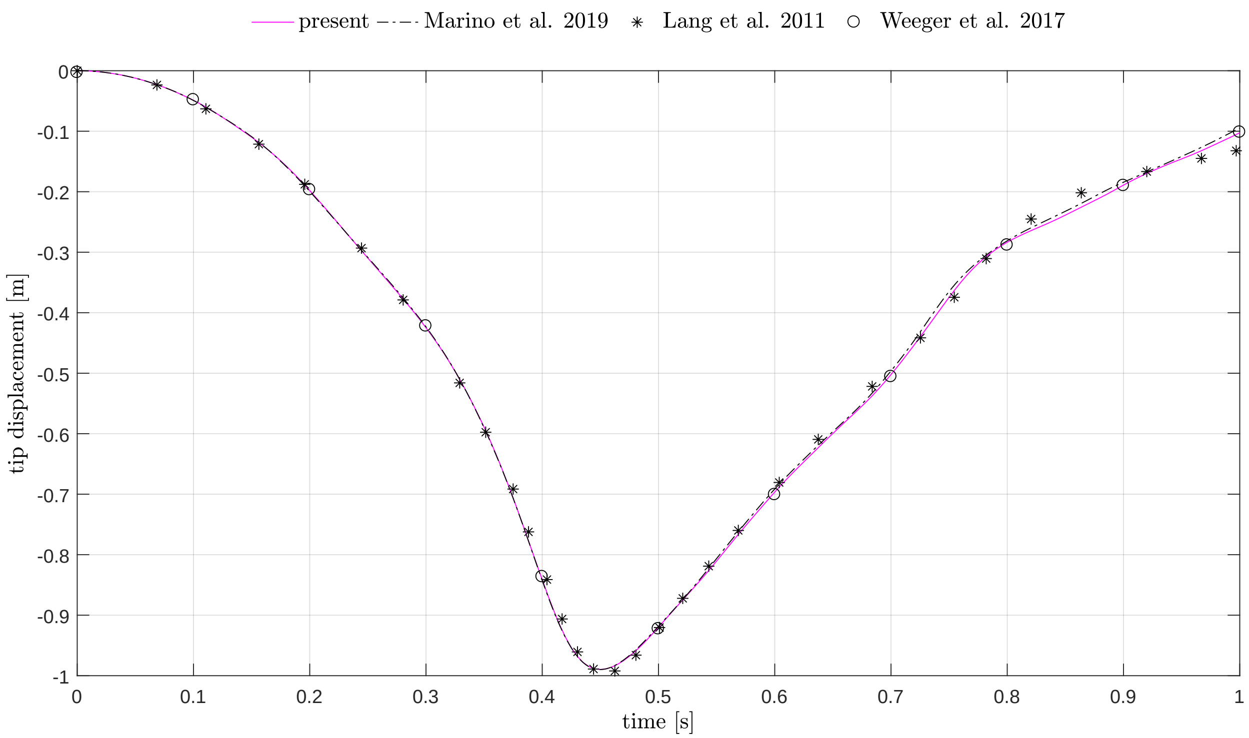

Figure 3: Vertical tip displacement of a swinging flexible pendulum. Comparisons are made with results obtained in Marino et al 2019 [34], Lang et al 2011 [46] and Weeger et al 2017 [33]. Results of the present formulation are obtained with $p = 6$, n $= 30$, $h = 5 \times 10^{-3}\,$s.

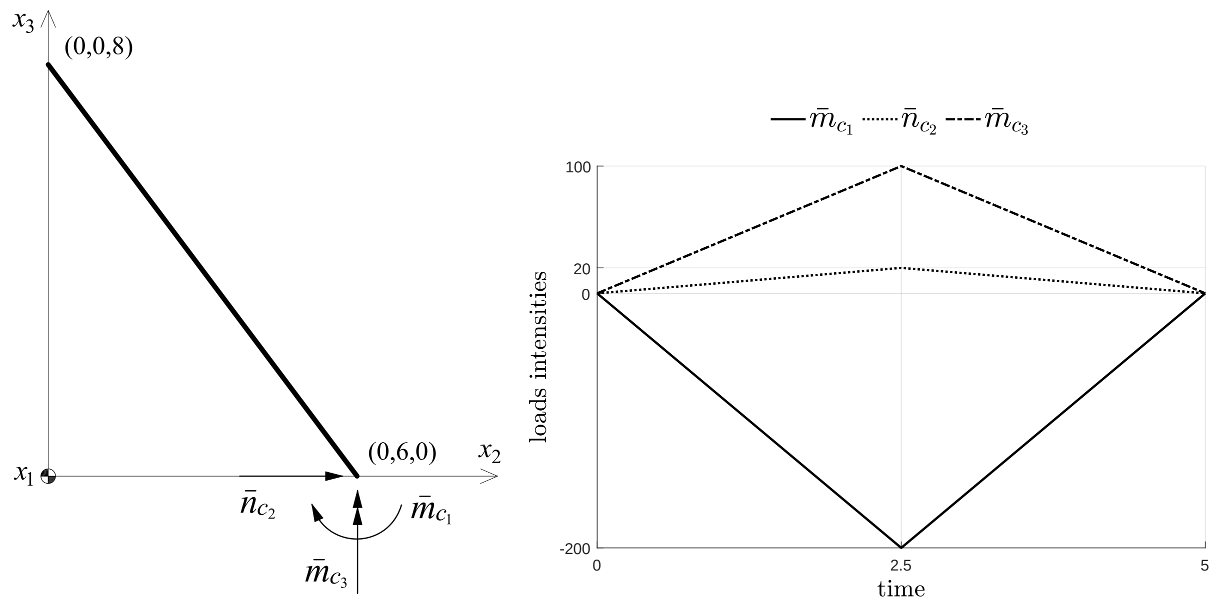

(a) Flying flexible beam subjected to tip force and moments.

(b) Loads time histories for the flying flexible beam.

Figure 4: Flying flexible beam: initial configuration and loads.

proposed originally by Simo & Vu-Quoc in [36] and later studied also in [48, 49, 53, 69, 70], consists of an initially straight free beam with length $L = 10$ placed in the plane (x_2, x_3) (see Figure 4(a)) subjected at the lower end to three different time-varying concentrated loads applied simultaneously (see Figure 4(b)). Under these loads the beam undergoes a forward translation due to $\bar{n}_{c_2}$, a forward tumbling due to $\bar{m}_{c_1}$ and an out-of-plane deformation due to $\bar{m}_{c_3}$.

First we test the high order accuracy of the formulation. The convergence curves of the L_2 norm of the error evaluated at $t = 2\,\mathrm{s}$ vs. the number of collocation points are shown in Figure 5. The error is calculated as $err_{L_2} = ||\boldsymbol{u}^r - \boldsymbol{u}^h||_{L_2}/||\boldsymbol{u}^r||_{L_2}$, where $\boldsymbol{u}^h$ and $\boldsymbol{u}^r$ are the approximate and reference displacements, respectively. The reference solution $\boldsymbol{u}^r$ is obtained with $p = 8$, n $= 200$ (approximately 2.3 on the abscissa of Figure 5) and $h = 0.1$. Very good convergence rates are observed up to $p = 5$. They are p for even degrees and $p-1$ for odd degrees, which is the typical behavior in isogeometric collocation using Greville points [1, 2, 30]. For higher degrees, especially for $p = 8$, as the number of collocation points increases, the temporal error becomes dominant and slightly affects the quality of the convergence rate.

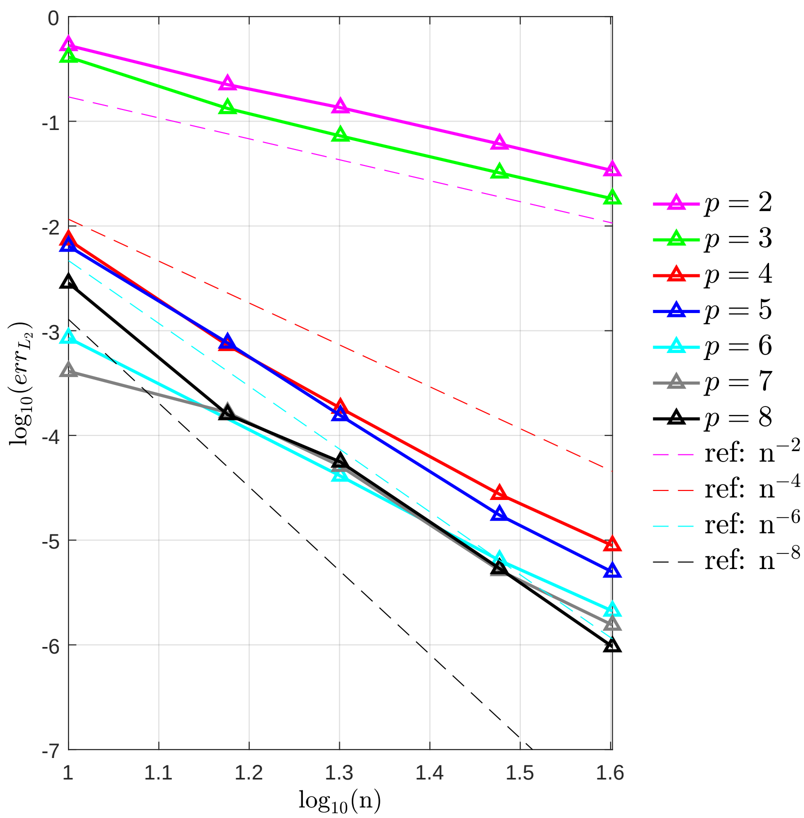

Figure 5: L_2 norm of the error evaluated at $t = 2\,\mathrm{s}$ vs. the number of collocation points for the free flying beam for NURBS basis functions of degrees $p = 2, \ldots, 8$. Dashed lines indicate reference orders of convergence. Reference solution computed with $p = 8$, $\mathrm{n} = 200$, $h = 0.1$.

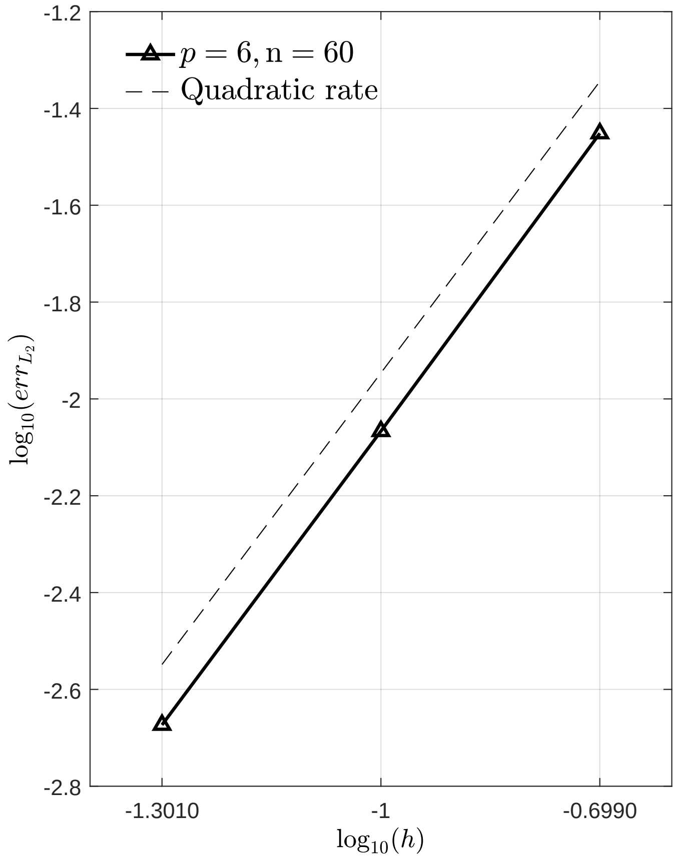

Figure 6: L_2 norm of the error vs. time step sizes of 0.05, 0.1, 0.2 for the free flying beam. The error is evaluated by comparing the beam configuration at $t = 5$ with a reference solution obtained with $h = 0.01$. In all cases $p = 6$ and $\mathrm{n} = 60$.

With our choice of β and γ, the standard Newmark time integration scheme is second-order accurate in time [36]. To verify that this attribute is preserved in the present IGA-C formulation on SO(3), we show in Figure 6 the error in L_2 norm associated with time step sizes of 0.05, 0.1, and 0.2. The error is evaluated by comparing the beam configuration at $t = 5$ with a reference solution obtained with $h = 0.01$. In all cases $p = 6$ and $\mathrm{n} = 60$. A perfectly quadratic rate is observed.

The correctness of the linearization procedure and the construction of the tangent matrix is confirmed by the convergence curves of the L_2 norm of the incremental vector during the iterations of the Newton-Raphson algorithm shown in Figure 7. Two cases are considered:

one with with $h = 0.1$ (left panel) and one with $h = 0.2$ (right panel). Both simulations are performed with $p = 6\,, \mathrm{n} = 60$ and are 5 time units long. The color of the curves shades from light gray (initial time steps) to darker gray (last time steps). Second order convergence rate is observed for all time instants and for both time step sizes. With $h = 0.1$ the tolerance of 10^{-10} is reached always in four iterations, whereas with $h = 0.2$ for some time steps five iterations are needed to achieve the same tolerance. When at the $(k+1)$th iteration the norm of the incremental vector is already pretty small (around 10^{-9}), at the next iteration a lower bound around 10^{-12} is observed. This bound is due to multiple reasons, such as the truncation error of the series used to express the derivatives of the exponential map involved in the beam curvature and its derivative (see Section 6.1) and the effect of the condition number on the machine precision.

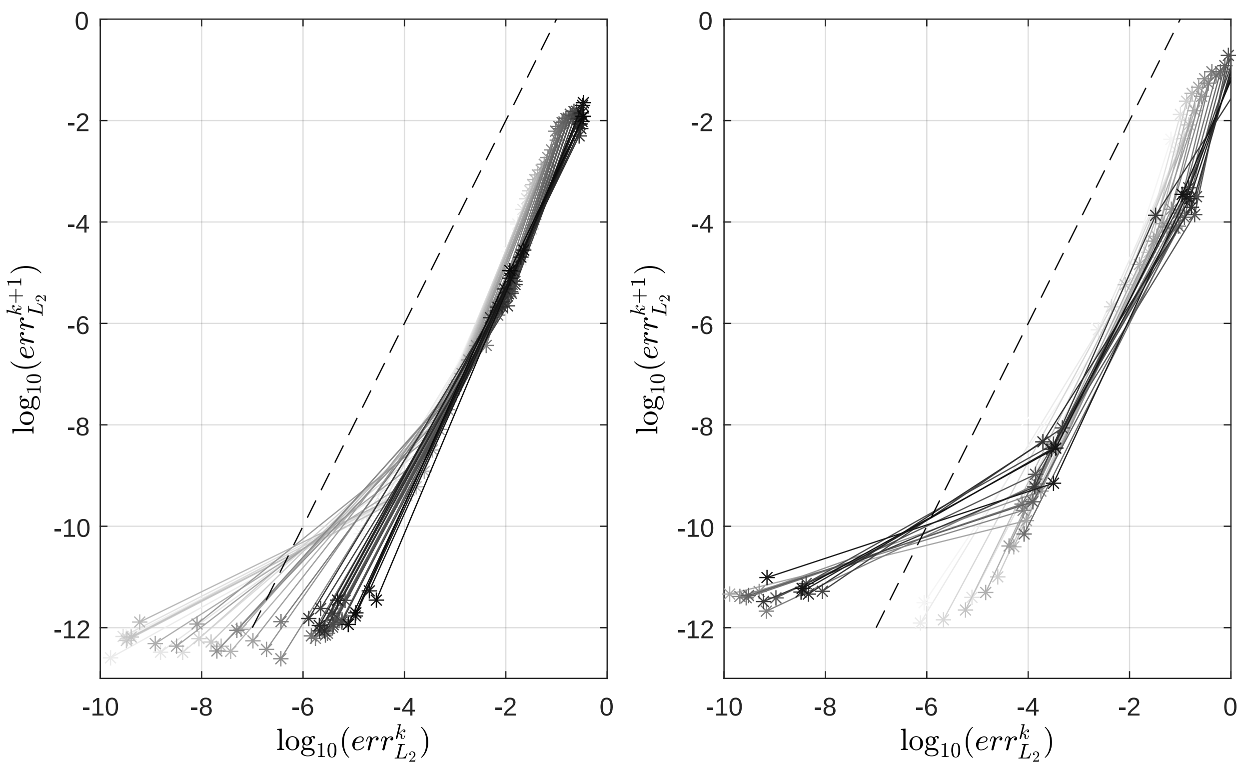

(a) Time step size $h = 0.1$ (50 curves).

(b) Time step size $h = 0.2$ (25 curves).

Figure 7: Convergence curves of the L_2 norm of the incremental vector during the Newton-Raphson iterations. The color of the curves shades from light gray (initial time steps) to darker gray (last time steps). Dashed line indicates the quadratic reference rate. Both simulations are obtained with $p = 6\,, \mathrm{n} = 60$. Total simulation time equals 5.

Figures 8 and 9 show some snapshots of the beam centroid line projected on the (x_2, x_3) and (x_1, x_3) planes, respectively; a three-dimensional view is shown in Figure 10. In all the figures, results associated with five combinations of p and h are shown. Note that in some cases snapshots at slightly different time instants with respect to [36] have been selected since we considered, in addition to $h = 0.1$, the case with $h = 0.2$. When the largest time step is considered ($h = 0.2$), as expected, the temporal error dominates the spatial one. Reducing the time step size to 0.1, the accuracy increases significantly. The beneficial effect of $p = 6$ over $p = 4$ for both time steps can be qualitatively appreciated at a magnified scale (see Figure 9).

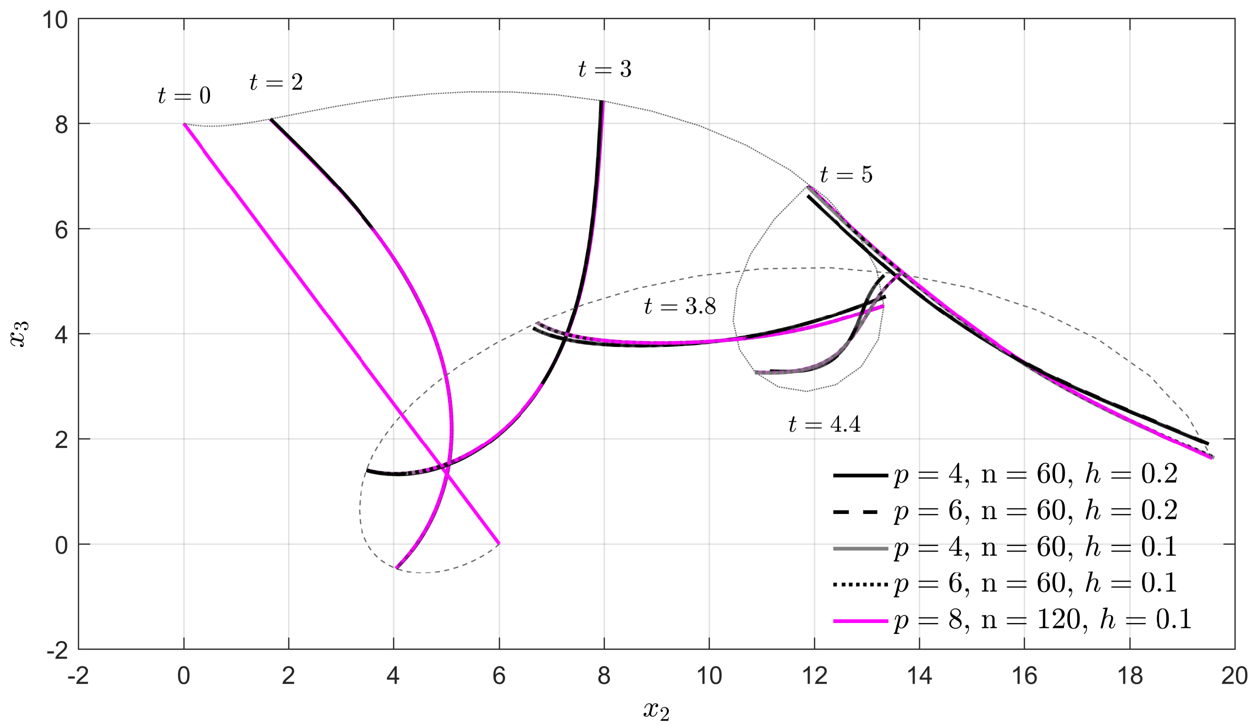

Figure 8: Snapshots of the free flying beam in the early tumbling stage projected on the (x_2, x_3) plane for different combinations of polynomial degrees, number of collocation points, and time step sizes. Gray dashed and dotted lines indicate the trajectories of the beam end points.

Figure 11 shows the material stress resultants $\boldsymbol{N}$ and $\boldsymbol{M}$ (see Eq. (9)) at $t = 2.5$ for $p = 6$, n = 60, $h = 0.1$. No oscillatory behavior is observed and almost identical results have been obtained with more refined meshes as well as with smaller time step sizes (these results are not reported here as they are almost indistinguishable in the figure). The good convergence

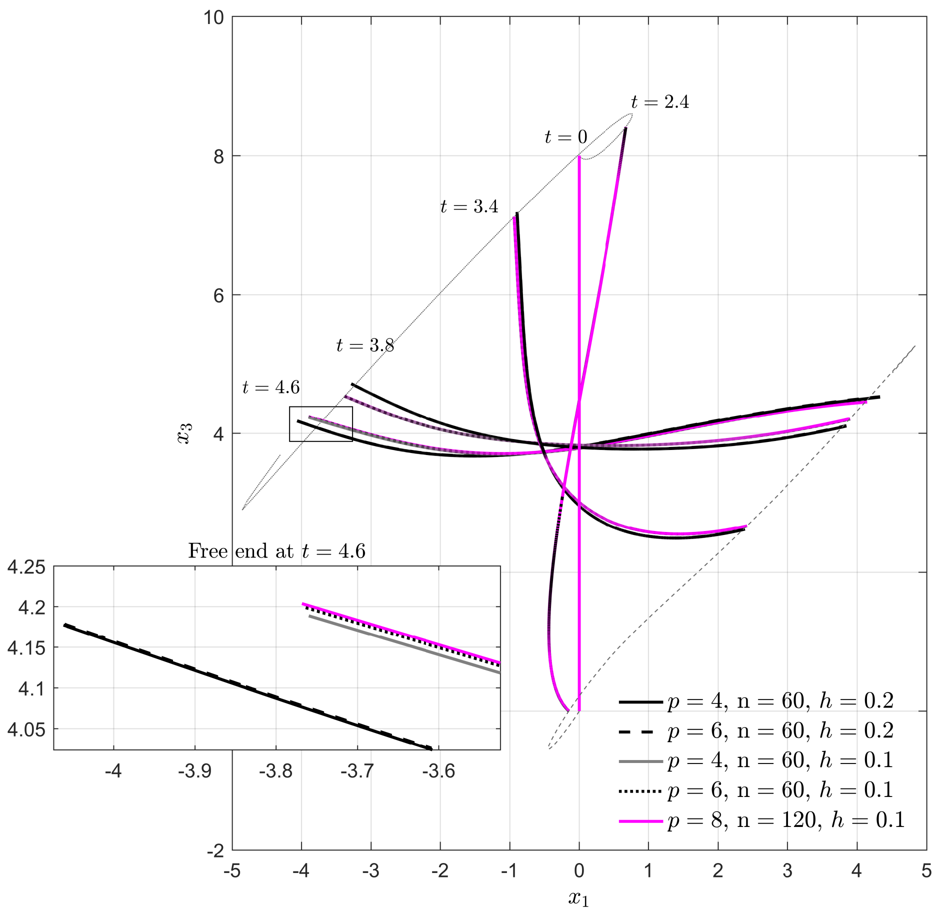

Figure 9: Snapshots of the free flying beam in the early tumbling stage projected on the (x_1, x_3) plane for different combinations of polynomial degrees, number of collocation points, and time step sizes. Gray dashed lines indicate the trajectories of the beam end points.

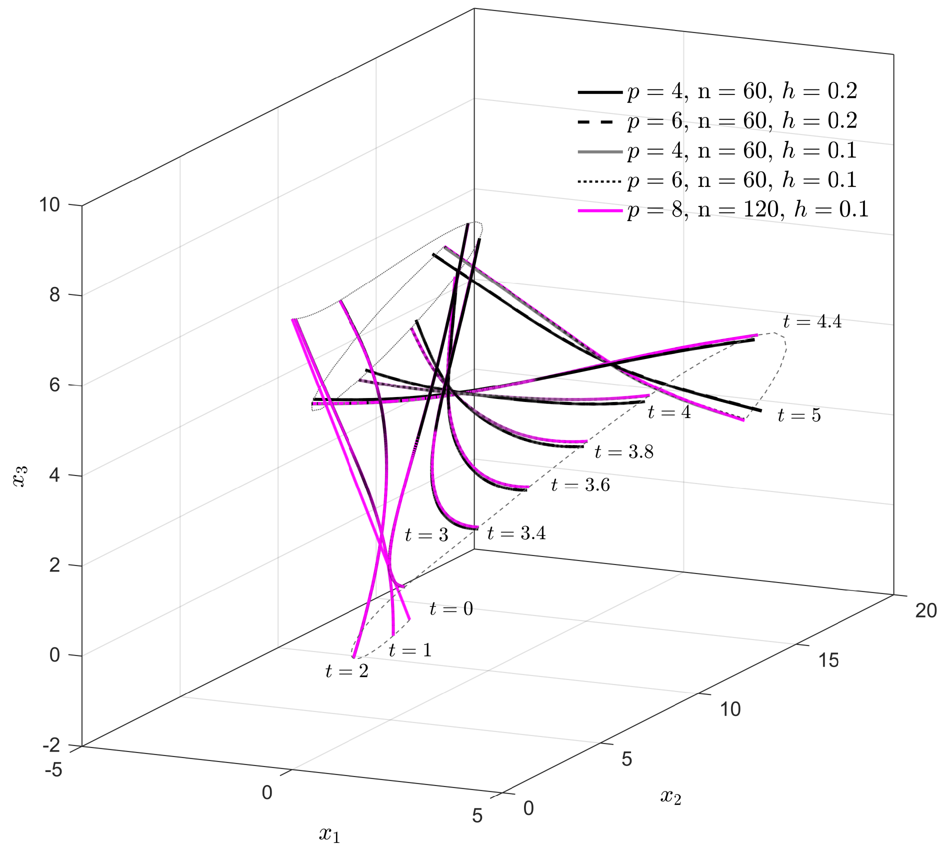

Figure 10: Snapshots of the free flying beam in the early tumbling stage in a three-dimensional view for different combinations of polynomial degrees, number of collocation points, and time step sizes. Gray dashed and dotted lines indicate the trajectories of the beam end points.

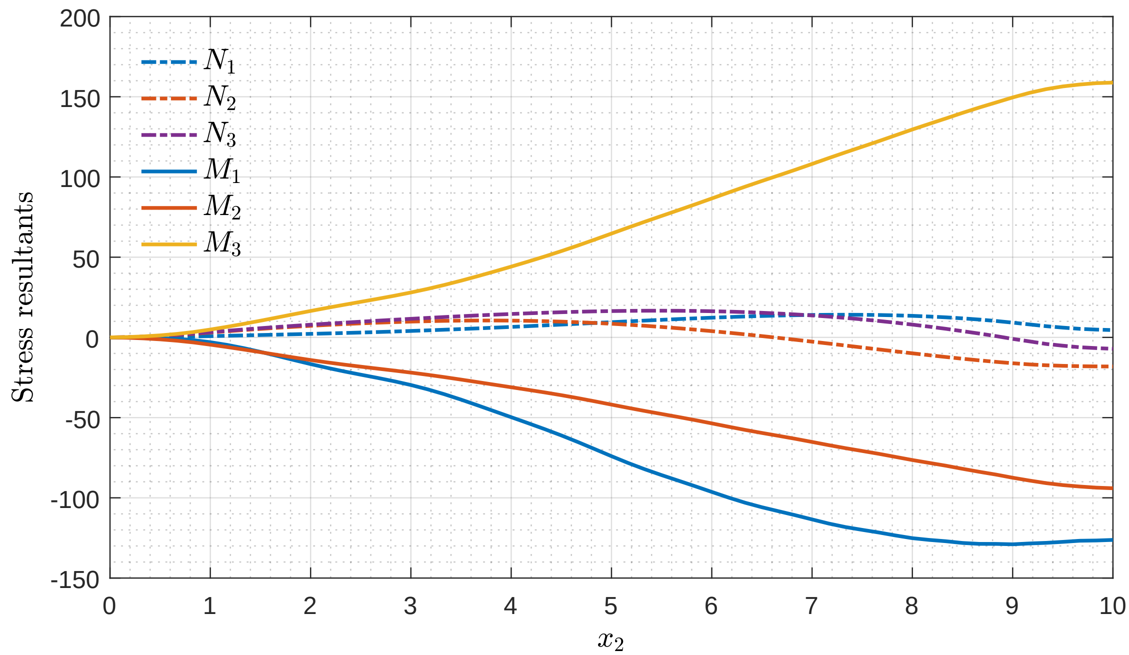

Figure 11: Free flying beam: stress resultants ($\boldsymbol{N}, \boldsymbol{M}$, see Eq. (9)) at $t = 2.5$ (maximum load intensities) over the beam length in the material setting.

rates observed in Figure 5 along with the smooth behavior of the stress resultants indicate that the results are not affected by locking effects.

Note that at $x_2 = 10$ and at time $t = 2.5$ the stress resultants shown in Figure 11, once rotated to the spatial setting through $\bar{\boldsymbol{n}} = \mathbf{R}\boldsymbol{N}$ and $\bar{\boldsymbol{m}} = \mathbf{R}\boldsymbol{M}$, coincide with the assigned loads given in Figure 4(b).

The performance of the formulation is also assessed for long simulations. Different views of a series of configurations taken with time increments of 0.1 up to a final time of 11.5 are shown in Figure 12.

Finally, we remark that the investigation of conserving properties is out of the scope of the present paper. However, since the Newmark scheme does not conserve energy nor momentum, loss of accuracy may occur for long-term simulations. The study of energy preserving schemes for nonlinear beams, see for example [43, 53, 71–75], is definitely an important direction for the future developments of this work.

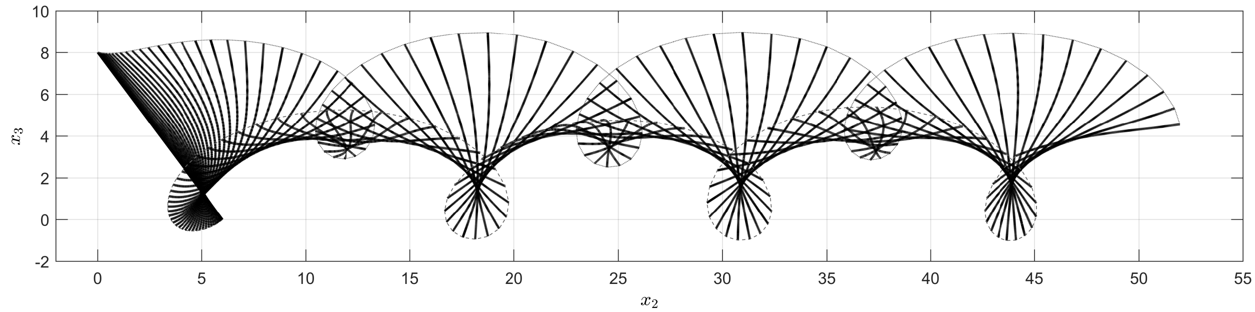

(a) Projections on the (x_2, x_3) plane.

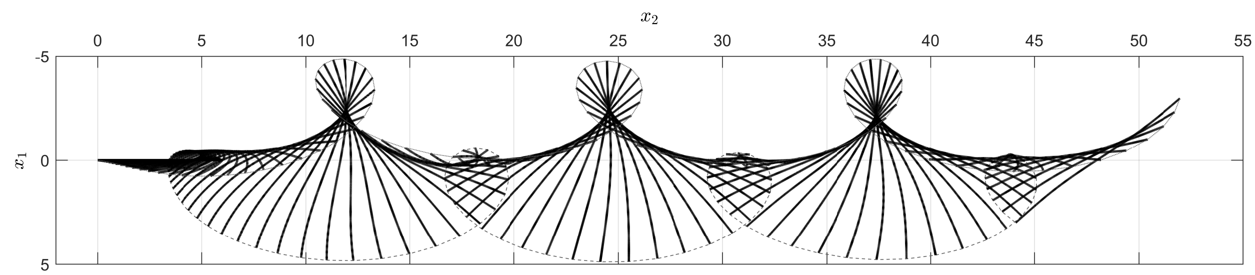

(b) Projections on the (x_1, x_2) plane.

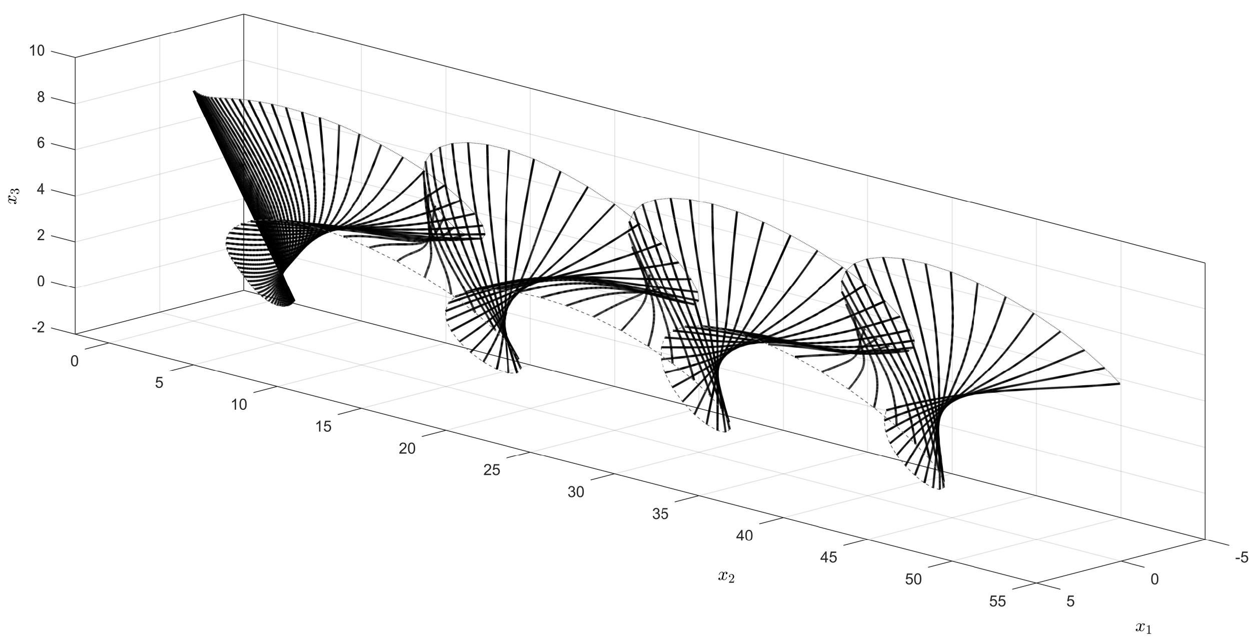

(c) Three-dimensional view with observer at $(135°, 15)$ (azimuth and vertical elevation).

Figure 12: Free flying beam: snapshots from time 0 to 11.5 with increments of 0.1.

8. Conclusions

With this paper we extended the field of applicability of the isogeometric collocation method to the dynamics of geometrically exact shear-deformable beams using a SO(3)-consistent version of the implicit Newmark scheme. The central issues of consistent linearization of the governing equations, variables initialization and update procedures are discussed in detail. In addition to very high stability, the proposed formulation ensures full consistency with the underlying geometric structure of the configuration manifold, is highly efficient due to the use of the rotation-vector parameterization, avoids the repetitive use of pull-backs and push-forwards since it is entirely formulated in the material setting, and is singularity free due to the use of the incremental rotation instead of the total rotation vector. We applied the proposed formulation to problems involving very large rotations and different boundary conditions. Correctness of the linearization and update procedures is proved by the quadratic convergence rate of the Newton-Raphson algorithm obtained in cases involving complex and large rotations even with a large time step size. In all cases a very good agreement with literature results is obtained. We observed that the method is stable and accurate also in cases where impulsive motions occur with loads applied without any ramp function. In addition, order elevation improves the overall accuracy significantly. In a context where efficiency is one of the major goals, this is a remarkable feature considering that order elevation is made at almost no additional computational cost. It is well known that the Newmark scheme does not conserve neither energy nor momentum and this can be a problem for long-term simulations. Future works should be oriented towards energy and momentum preserving methods with isogeometric collocation.

Acknowledgements

Josef Kiendl was supported by the Onsager fellowship program of NTNU. Laura De Lorenzis was supported by the DFG Priority Program SPP 1748 "Reliable Simulation Techniques in Solid Mechanics".

Appendix A. Directional derivatives

In this Appendix we provide the complete set of directional derivatives needed for the linearization of the governing equations discussed in Section 5. Directional derivatives are carried out using the incremental rotation vector $\delta\boldsymbol{\Theta}$ in the material form. Thus, this Appendix complements the formulas provided in Appendix A of [28], where the spatial form of the incremental rotation vector was used.

Directional derivative of $\boldsymbol{c}_{,s}$.

$$\frac{d}{d\varepsilon}\left(\boldsymbol{c}_{\varepsilon,s}\right)_{\varepsilon=0} = \frac{d}{d\varepsilon}\left[\left(\boldsymbol{c}+\varepsilon\delta\boldsymbol{\eta}\right)_{,s}\right]_{\varepsilon=0} = \delta\boldsymbol{\eta}_{,s}\ . \tag{A.1}$$

Directional derivative of $\boldsymbol{c}_{,ss}$.

$$\frac{d}{d\varepsilon}\left(\boldsymbol{c}_{\varepsilon,ss}\right)_{\varepsilon=0} = \delta\boldsymbol{\eta}_{,ss}\ . \tag{A.2}$$

Directional derivative of $\mathbf{R}$.

$$\frac{d}{d\varepsilon}\left(\mathbf{R}_{\varepsilon}\right)_{\varepsilon=0} = \frac{d}{d\varepsilon}\left(\mathbf{R}\exp(\varepsilon\delta\widetilde{\boldsymbol{\Theta}})\right)_{\varepsilon=0} = \mathbf{R}\delta\widetilde{\boldsymbol{\Theta}}\,. \tag{A.3}$$

Directional derivative of $\mathbf{R}^{\mathsf{T}}$.

$$\frac{d}{d\varepsilon}\left(\mathbf{R}_{\varepsilon}^{\mathsf{T}}\right)_{\varepsilon=0} = \frac{d}{d\varepsilon}\left(\exp(-\varepsilon\delta\widetilde{\boldsymbol{\Theta}})\mathbf{R}^{\mathsf{T}}\right)_{\varepsilon=0} = -\delta\widetilde{\boldsymbol{\Theta}}\mathbf{R}^{\mathsf{T}}\,. \tag{A.4}$$

Directional derivative of $\mathbf{R}_{,s}$.

$$\frac{d}{d\varepsilon}\left(\mathbf{R}_{\varepsilon,s}\right)_{\varepsilon=0} = \mathbf{R}\widetilde{\boldsymbol{K}}\delta\widetilde{\boldsymbol{\Theta}} + \mathbf{R}\delta\widetilde{\boldsymbol{\Theta}}_{,s}\ . \tag{A.5}$$

Directional derivative of $\mathbf{R}^{\mathsf{T}}{}_{,s}$.

$$\frac{d}{d\varepsilon}\left(\mathbf{R}_{\varepsilon,s}^{\mathsf{T}}\right)_{\varepsilon=0} = \delta\widetilde{\boldsymbol{\Theta}}\widetilde{\boldsymbol{K}}\mathbf{R}^{\mathsf{T}} - \delta\widetilde{\boldsymbol{\Theta}}_{,s}\mathbf{R}^{\mathsf{T}}\,. \tag{A.6}$$

Directional derivative of $\widetilde{\boldsymbol{K}}$. Making use of (A.4) and (A.5), we obtain

$$\frac{d}{d\varepsilon}\left(\widetilde{\boldsymbol{K}}_{\varepsilon}\right)_{\varepsilon=0} = \frac{d}{d\varepsilon}\left(\mathbf{R}_{\varepsilon}^{\mathsf{T}}\mathbf{R}_{\varepsilon,s}\right)_{\varepsilon=0} = [\widetilde{\boldsymbol{K}},\delta\widetilde{\boldsymbol{\Theta}}] + \delta\widetilde{\boldsymbol{\Theta}}_{,s}\ , \tag{A.7}$$

where the Lie bracket has been used $[\widetilde{\boldsymbol{K}},\delta\widetilde{\boldsymbol{\Theta}}] = \widetilde{\boldsymbol{K}}\delta\widetilde{\boldsymbol{\Theta}} - \delta\widetilde{\boldsymbol{\Theta}}\widetilde{\boldsymbol{K}}$.

The corresponding axial vector is found by exploiting the Jacobi identity $\left(\widetilde{\boldsymbol{K}}\delta\widetilde{\boldsymbol{\Theta}} - \delta\widetilde{\boldsymbol{\Theta}}\widetilde{\boldsymbol{K}}\right)\boldsymbol{h} = \widetilde{\boldsymbol{K}}\delta\boldsymbol{\Theta}\times\boldsymbol{h}$ for any $\boldsymbol{h}\in\mathbb{R}^3$, which leads to

$$\frac{d}{d\varepsilon}\left(\boldsymbol{K}_{\varepsilon}\right)_{\varepsilon=0} = \widetilde{\boldsymbol{K}}\delta\boldsymbol{\Theta} + \delta\boldsymbol{\Theta}_{,s}\ . \tag{A.8}$$

Directional derivative of $\mathbf{R}_{,ss}$.

$$\frac{d}{d\varepsilon}\left(\mathbf{R}_{\varepsilon,ss}\right)_{\varepsilon=0}=\mathbf{R}\left(\widetilde{\boldsymbol{K}}^{2}+\widetilde{\boldsymbol{K}}_{,s}\right)\delta\widetilde{\boldsymbol{\Theta}}+2\mathbf{R}\widetilde{\boldsymbol{K}}\widetilde{\boldsymbol{\Theta}}_{,s}+\mathbf{R}\delta\widetilde{\boldsymbol{\Theta}}_{,ss}\ . \tag{A.9}$$

Directional derivative of $\boldsymbol{K}_{,s}$. We start with the derivative of $\widetilde{\boldsymbol{K}}_{,s}$ and recall that

$$\widetilde{\boldsymbol{K}}_{\varepsilon,s}=(\mathbf{R}_{\varepsilon}^{\mathsf{T}}\mathbf{R}_{\varepsilon,s})_{,s}=\mathbf{R}_{\varepsilon,s}^{\mathsf{T}}\mathbf{R}_{\varepsilon,s}+\mathbf{R}_{\varepsilon}^{\mathsf{T}}\mathbf{R}_{\varepsilon,ss}\ , \tag{A.10}$$

from which, by making use of equations (A.6), (A.5), (A.4), and (A.9), and after some manipulations, we obtain

$$\frac{d}{d\varepsilon}\left(\widetilde{\boldsymbol{K}}_{\varepsilon,s}\right)_{\varepsilon=0}=\left[\widetilde{\boldsymbol{K}},\delta\widetilde{\boldsymbol{\Theta}}_{,s}\right]+\left[\widetilde{\boldsymbol{K}}_{,s}\,,\delta\widetilde{\boldsymbol{\Theta}}\right]+\delta\widetilde{\boldsymbol{\Theta}}_{,ss}\ , \tag{A.11}$$

where again the Lie bracket have been used.

Again, by exploiting the Jacobi identity, the corresponding axial vector is obtained as follows

$$\frac{d}{d\varepsilon}\left(\boldsymbol{K}_{\varepsilon,s}\right)_{\varepsilon=0}=\widetilde{\boldsymbol{K}}\delta\boldsymbol{\Theta}_{,s}+\widetilde{\boldsymbol{K}}_{,s}\,\delta\boldsymbol{\Theta}+\delta\boldsymbol{\Theta}_{,ss}\ . \tag{A.12}$$

Directional derivative of $\boldsymbol{\Gamma}_N$. Making use of (A.4) and (A.1), it follows that

$$\frac{d}{d\varepsilon}\left(\boldsymbol{\Gamma}_{N\varepsilon}\right)_{\varepsilon=0}=\frac{d}{d\varepsilon}\left(\boldsymbol{\Gamma}_{\varepsilon}-\boldsymbol{\Gamma}_{0}\right)_{\varepsilon=0}=\mathbf{R}^{\mathsf{T}}\boldsymbol{\eta}_{,s}+(\widetilde{\mathbf{R}^{\mathsf{T}}\boldsymbol{c}_{,s}})\delta\boldsymbol{\Theta}\,. \tag{A.13}$$

Directional derivative of $\boldsymbol{\Gamma}_{N,s}$.

$$\frac{d}{d\varepsilon}\left(\boldsymbol{\Gamma}_{N\varepsilon,s}\right)_{\varepsilon=0}=\left(-\delta\widetilde{\boldsymbol{\Theta}}_{,s}+\delta\widetilde{\boldsymbol{\Theta}}\widetilde{\boldsymbol{K}}\right)\mathbf{R}^{\mathsf{T}}\boldsymbol{c}_{,s}-\widetilde{\boldsymbol{K}}\mathbf{R}^{\mathsf{T}}\boldsymbol{\eta}_{,s}-\delta\widetilde{\boldsymbol{\Theta}}\mathbf{R}^{\mathsf{T}}\boldsymbol{c}_{,ss}-\mathbf{R}^{\mathsf{T}}\boldsymbol{\eta}_{,ss}\ . \tag{A.14}$$

References

[1] F. Auricchio, L. Beirão Da Veiga, T. J. R. Hughes, A. Reali, G. Sangalli, Isogeometric Collocation Methods, Mathematical Models and Methods in Applied Sciences 20 (11) (2010) 2075–2107.

[2] F. Auricchio, L. Beirão da Veiga, T. J. R. Hughes, A. Reali, G. Sangalli, Isogeometric collocation for elastostatics and explicit dynamics, Computer Methods in Applied Mechanics and Engineering 249-252 (2012) 2–14.

[3] T. Hughes, J. Cottrell, Y. Bazilevs, Isogeometric analysis: CAD, finite elements, NURBS, exact geometry and mesh refinement, Computer Methods in Applied Mechanics and Engineering 194 (39-41) (2005) 4135–4195.

[4] J. A. Cottrell, T. J. R. Hughes, Y. Bazilevs, Isogeometric analysis: toward integration of CAD and FEA, JohnWiley & Sons, Ltd Registered, 2009.

[5] Y. Bazilevs, L. Beirão da Veiga, J. Cottrell, T. J. R. Hughes, G. Sangalli, Isogeometric analysis: approximation, stability and error estimates for h-refined meshes, Mathematical Models and Methods in Applied Sciences 16 (07) (2006) 1031–1090.

[6] T. J. R. Hughes, A. Reali, G. Sangalli, Duality and unified analysis of discrete approximations in structural dynamics and wave propagation: Comparison of p-method finite elements with k-method NURBS, Computer Methods in Applied Mechanics and Engineering 197 (49-50) (2008) 4104–4124.

[7] J. A. Evans, Y. Bazilevs, I. Babuška, T. J. R. Hughes, n-Widths, supinfs, and optimality ratios for the k-version of the isogeometric finite element method, Computer Methods in Applied Mechanics and Engineering 198 (21-26) (2009) 1726–1741.

[8] L. Beirão da Veiga, A. Buffa, J. Rivas, G. Sangalli, Some estimates for h-p-k-refinement in isogeometric analysis., Numerische Mathematik 118 (2011) 271–305.

[9] C. Adam, T. J. R. Hughes, S. Bouabdallah, M. Zarroug, H. Maitournam, Selective and reduced numerical integrations for NURBS-based isogeometric analysis, Computer Methods in Applied Mechanics and Engineering 284 (2015) 732–761.

[10] P. Antolin, A. Buffa, F. Calabrò, M. Martinelli, G. Sangalli, Efficient matrix computation for tensor-product isogeometric analysis: The use of sum factorization, Computer Methods in Applied Mechanics and Engineering 285 (2015) 817–828.

[11] F. Calabrò, G. Sangalli, M. Tani, Fast formation of isogeometric Galerkin matrices by weighted quadrature, Computer Methods in Applied Mechanics and Engineering 316 (2017) 606–622.

[12] F. Fahrendorf, L. De Lorenzis, H. Gomez, Reduced integration at superconvergent points in isogeometric analysis, Computer Methods in Applied Mechanics and Engineering 328 (2018) 390–410.

[13] G. Sangalli, M. Tani, Matrix-free weighted quadrature for a computationally efficient isogeometric k-method, Computer Methods in Applied Mechanics and Engineering 338 (2018) 117–133.

[14] D. Schillinger, J. Evans, A. Reali, M. Scott, T. J. R. Hughes, Isogeometric collocation: Cost comparison with Galerkin methods and extension to adaptive hierarchical NURBS discretizations, Computer Methods in Applied Mechanics and Engineering 267 (2013) 170–232.

[15] H. Gomez, A. Reali, G. Sangalli, Accurate, efficient, and (iso)geometrically flexible collocation methods for phase-field models., Journal for Computational Physics 262 (2014) 153–171.

[16] L. De Lorenzis, J. Evans, T. Hughes, A. Reali, Isogeometric collocation: Neumann boundary conditions and contact, Computer Methods in Applied Mechanics and Engineering 284 (2015) 21–54.

[17] R. Kruse, N. Nguyen-Thanh, L. De Lorenzis, T. Hughes, Isogeometric collocation for large deformation elasticity and frictional contact problems, Computer Methods in Applied Mechanics and Engineering 296 (2015) 73–112.

[18] H. Gomez, L. De Lorenzis, The variational collocation method, Computer Methods in Applied Mechanics and Engineering 309 (2016) 152–181.

[19] L. Beirão da Veiga, C. Lovadina, a. Reali, Avoiding shear locking for the Timoshenko beam problem via isogeometric collocation methods, Computer Methods in Applied Mechanics and Engineering 241-244 (2012) 38–51.

[20] F. Auricchio, L. Beirão da Veiga, J. Kiendl, C. Lovadina, a. Reali, Locking-free isogeometric collocation methods for spatial Timoshenko rods, Computer Methods in Applied Mechanics and Engineering 263 (2013) 113–126.

[21] J. Kiendl, F. Auricchio, T. Hughes, A. Reali, Single-variable formulations and isogeometric discretizations for shear deformable beams, Computer Methods in Applied Mechanics and Engineering 284 (2015) 988–1004.

[22] J. Kiendl, F. Auricchio, A. Reali, A displacement-free formulation for the Timoshenko beam problem and a corresponding isogeometric collocation approach, Meccanica (2017) 1–11.

[23] G. Balduzzi, S. Morganti, F. Auricchio, Non-prismatic Timoshenko-like beam model: Numerical solution via isogeometric collocation, Computers & Mathematics with Applications 74 (7) (2017) 1531–1541.

[24] A. Reali, H. Gomez, An isogeometric collocation approach for Bernoulli-Euler beams and Kirchhoff plates, Computer Methods in Applied Mechanics and Engineering 284 (2015) 623–636.

[25] J. Kiendl, F. Auricchio, L. Beirão da Veiga, C. Lovadina, A. Reali, Isogeometric collocation methods for the Reissner-Mindlin plate problem, Computer Methods in Applied Mechanics and Engineering 284 (2015) 489–507.

[26] J. Kiendl, E. Marino, L. De Lorenzis, Isogeometric collocation for the Reissner-Mindlin shell problem, Computer Methods in Applied Mechanics and Engineering 325 (2017) 645–665.

[27] F. Maurin, F. Greco, L. Coox, D. Vandepitte, W. Desmet, Isogeometric collocation for Kirchhoff-Love plates and shells, Computer Methods in Applied Mechanics and Engineering 329 (2018) 396–420.

[28] E. Marino, Isogeometric collocation for three-dimensional geometrically exact shear-deformable beams, Computer Methods in Applied Mechanics and Engineering 307 (2016) 383–410.

[29] O. Weeger, S.-K. Yeung, M. L. Dunn, Isogeometric collocation methods for Cosserat rods and rod structures, Computer Methods in Applied Mechanics and Engineering 316 (2017) 100–122.

[30] E. Marino, Locking-free isogeometric collocation formulation for three-dimensional geometrically exact shear-deformable beams with arbitrary initial curvature, Computer Methods in Applied Mechanics and Engineering 324 (2017) 546–572.

[31] F. Maurin, F. Greco, S. Dedoncker, W. Desmet, Isogeometric analysis for nonlinear planar Kirchhoff rods: Weighted residual formulation and collocation of the strong form, Computer Methods in Applied Mechanics and Engineering.

[32] J. A. Evans, R. R. Hiemstra, T. J. R. Hughes, A. Reali, Explicit higher-order accurate isogeometric collocation methods for structural dynamics, Computer Methods in Applied Mechanics and Engineering 338 (2018) 208–240.

[33] O. Weeger, B. Narayanan, M. L. Dunn, Isogeometric collocation for nonlinear dynamic analysis of Cosserat rods with frictional contact, Nonlinear Dynamics (2017) 1–15.

[34] E. Marino, J. Kiendl, L. De Lorenzis, Explicit isogeometric collocation for the dynamics of three-dimensional beams undergoing finite motions, Computer Methods in Applied Mechanics and Engineering 343 (2019) 530–549.

[35] Y. Choquet-Bruhat, C. Dewitt-Morette, Analysis, manifolds and physics Part I: Basics, Elsevier B.V., 1996.

[36] J. C. Simo, L. Vu-Quoc, On the dynamics in space of rods undergoing large motions A geometrically exact approach, Computer Methods in Applied Mechanics and Engineering 66 (2) (1988) 125–161.

[37] J. Mäkinen, Rotation manifold SO(3) and its tangential vectors, Computational Mechanics 42 (6) (2008) 907–919.

[38] A. Cardona, M. Geradin, A beam finite element non-linear theory with finite rotations, International Journal for Numerical Methods in Engineering 26 (September 1987) (1988) 2403–2438.

[39] A. Ibrahimbegović, M. A. L. Mikdad, Finite rotations in dynamics of beams and implicit time-stepping schemes, International Journal for Numerical Methods in Engineering 41 (November 1996) (1998) 781–814.

[40] G. Jelenic, M. A. Crisfield, Interpolation of Rotational Variables in Nonlinear Dynamics of 3D Beams, International Journal for Numerical Methods in Engineering 1222 (February 1997) (1998) 1193–1222.

[41] G. Jelenić, M. Crisfield, Geometrically exact 3D beam theory: implementation of a strain-invariant finite element for statics and dynamics, Computer Methods in Applied Mechanics and Engineering 171 (1-2) (1999) 141–171.

[42] J. Mäkinen, Critical study of Newmark-scheme on manifold of finite rotations, Computer Methods in Applied Mechanics and Engineering 191 (2001) 817–828.

[43] I. Romero, F. Armero, An objective finite element approximation of the kinematics of geometrically exact rods and its use in the formulation of an energy-momentum conserving scheme in dynamics, International Journal for Numerical Methods in Engineering 54 (12) (2002) 1683–1716.

[44] J. Mäkinen, Total Lagrangian Reissner's geometrically exact beam element without singularities, International Journal for Numerical Methods in Engineering 70 (October 2006) (2007) 1009–1048.

[45] P. M. Pimenta, E. M. B. Campello, P. Wriggers, An exact conserving algorithm for nonlinear dynamics with rotational DOFs and general hyperelasticity. Part 1: Rods, Computational Mechanics 42 (5) (2008) 715–732.

[46] H. Lang, J. Linn, M. Arnold, Multi-body dynamics simulation of geometrically exact Cosserat rods, Multibody System Dynamics 25 (3) (2011) 285–312.

[47] O. Brüls, A. Cardona, M. Arnold, Lie group generalized-α time integration of constrained flexible multibody systems, Mechanism and Machine Theory 48 (2012) 121–137.

[48] E. Zupan, M. Saje, D. Zupan, Quaternion-based dynamics of geometrically nonlinear spatial beams using the RungeKutta method, Finite Elements in Analysis and Design 54 (2012) 48–60.

[49] E. Zupan, M. Saje, D. Zupan, Dynamics of spatial beams in quaternion description based on the Newmark integration scheme, Computational Mechanics 51 (1) (2013) 47–64.

[50] V. Sonneville, A. Cardona, O. Brüls, Geometrically exact beam finite element formulated on the special Euclidean group SE(3), Computer Methods in Applied Mechanics and Engineering 268 (3) (2014) 451–474.

[51] T.-N. Le, J.-M. Battini, M. Hjiaj, A consistent 3D corotational beam element for nonlinear dynamic analysis of flexible structures, Computer Methods in Applied Mechanics and Engineering 269 (2014) 538–565.

[52] P. M. Almonacid, Explicit symplectic momentum-conserving time-stepping scheme for the dynamics of geometrically exact rods, Finite Elements in Analysis and Design 96 (2015) 11–22.

[53] E. Zupan, D. Zupan, On conservation of energy and kinematic compatibility in dynamics of nonlinear velocity-based three-dimensional beams, Nonlinear Dynamics 95 (2) (2019) 1379–1394.

[54] J. Stuelpnagel, On the Parametrization of the Three-Dimensional Rotation Group, SIAM Review 6 (4) (1964) 422–430.

[55] J. Argyris, An excursion into large rotations, Computer Methods in Applied Mechanics and Engineering 32 (13) (1982) 85–155.

[56] H. Cheng, K. C. Gupta, An Historical Note on Finite Rotations, Journal of Applied Mechanics 56 (1) (1989) 139.

[57] J. E. Marsden, T. S. Ratiu, Introduction to Mechanics and Symmetry, 2nd Edition, Texts in Applied Mathematics, Springer, New York, NY, 1999.

[58] J. C. Simo, A finite strain beam formulation. The three-dimensional dynamic problem. Part I, Computer Methods in Applied Mechanics and Engineering 49 (1) (1985) 55–70.

[59] M. A. Crisfield, G. Jelenić;, Objectivity of strain measures in the geometrically exact three-dimensional beam theory and its finite-element implementation, Proceedings of the Royal Society of London A: Mathematical, Physical and Engineering Sciences 455 (1983) (1999) 1125–1147.

[60] R. K. Kapania, J. Li, On a geometrically exact curved/twisted beam theory under rigid cross-section assumption, Computational Mechanics 30 (5-6) (2003) 428–443.

[61] J. C. Simo, L. Vu-Quoc, A three-dimensional finite-strain rod model. Part II: Computational aspects, Computer Methods in Applied Mechanics and Engineering 58 (1) (1986) 79–116.

[62] J. C. Simo, K. K. Wong, Unconditionally stable algorithms for rigid body dynamics that exactly preserve energy and momentum, International Journal for Numerical Methods in Engineering 31 (1) (1991) 19–52.

[63] C. Anitescu, Y. Jia, Y. J. Zhang, T. Rabczuk, An isogeometric collocation method using superconvergent points, Computer Methods in Applied Mechanics and Engineering 284 (2015) 1073–1097.

[64] M. Montardini, G. Sangalli, L. Tamellini, Optimal-order isogeometric collocation at Galerkin superconvergent points, Computer Methods in Applied Mechanics and Engineering 316 (2017) 741–757.

[65] Y. Jia, C. Anitescu, Y. J. Zhang, T. Rabczuk, An adaptive isogeometric analysis collocation method with a recovery-based error estimator, Computer Methods in Applied Mechanics and Engineering 345 (2019) 52–74.

[66] W. Rossmann, Lie groups An Introduction Through Linear Groups, Oxford University Press, 2002.

[67] R. A. Spurrier, Comment on ”Singularity-Free Extraction of a Quaternion from a Direction-Cosine Matrix&quot”, Journal of Spacecraft and Rockets 15 (4) (1978) 255–255.

[68] A. Gravouil, A. Combescure, Multi-time-step explicit-implicit method for non-linear structural dynamics, International Journal for Numerical Methods in Engineering 50 (1) (2001) 199–225.

[69] K. M. Hsiao, J. Y. Lin, W. Y. Lin, A consistent co-rotational finite element formulation for geometrically nonlinear dynamic analysis of 3-D beams, Computer Methods in Applied Mechanics and Engineering 169 (1-2) (1999) 1–18.

[70] R. Zhang, H. Zhong, A quadrature element formulation of an energymomentum conserving algorithm for dynamic analysis of geometrically exact beams, Computers \& Structures 165 (2016) 96–106.

[71] J. C. Simo, N. Tarnow, M. Doblare, Non-linear dynamics of three-dimensional rods: Exact energy and momentum conserving algorithms, International Journal for Numerical Methods in Engineering 38 (9) (1995) 1431–1473.

[72] C. L. Bottasso, M. Borri, Energy preserving/decaying schemes for non-linear beam dynamics using the helicoidal approximation, Computer Methods in Applied Mechanics and Engineering 143 (3-4) (1997) 393–415.

[73] A. Ibrahimbegovic, R. L. Taylor, On the role of frame-invariance in structural mechanics models at finite rotations, Computer Methods in Applied Mechanics and Engineering 191 (45) (2002) 5159–5176.

[74] S. Leyendecker, P. Betsch, P. Steinmann, Objective energymomentum conserving integration for the constrained dynamics of geometrically exact beams, Computer Methods in Applied Mechanics and Engineering 195 (19-22) (2006) 2313–2333.

[75] E. V. Lens, A. Cardona, A nonlinear beam element formulation in the framework of an energy preserving time integration scheme for constrained multibody systems dynamics, Computers & structures 86 (2008) 47–63.